Electron Impact Excitation of the X $^1\Sigma_g^+$ (v"=0) to the a″ $^1\Sigma_g^+$, the b$^1\Pi_u$, c$^1\Pi_u$, o$^1\Pi_u$, b′ $^1\Sigma_u^+$, c′ $^1\Sigma_u^+$, F $^3\Pi_u$ and G $^3\Pi_u$ states of Molecular Nitrogen.

Murtadha A Khakoo, Shi-Yang Wang, Vaasu Swaminathan, Daniel Nuyujukian

Department of Physics, California State University Fullerton, Fullerton, CA 92831, USA

Russ Laher,

Spitzer Science Center, California Institute of Technology, Pasadena, CA 91125

Brenton Lewis,

Australian National University, Canberra ACT 0200, Australia,

Paul V. Johnson, Charles P. Malone and Isik Kanik

Jet Propulsion Laboratory, California Institute of Technology, 4800 Oak Grove Drive, Pasadena, CA 91109, USA

New measurements of differential cross-sections (DCSs) for the excitation of the X $^1\Sigma_g^+$ (v″ = 0) → a″$^1\Sigma_g^+$, the b$^1\Pi_u$, c$^1\Pi_u$, o$^1\Pi_u$, b′ $^1\Sigma_u^+$ and c′ $^1\Sigma_u^+$ and the F $^3\Pi_u$ and G $^3\Pi_u$ transitions in N_2 are presented, in the energy loss region of 12.0eV to 13.82eV. The DCSs were obtained from energy loss spectra measured at incident energies of 17.5eV, 20eV, 30eV, 50eV and 100eV and for scattering angles ranging from 3° to 130°. The analysis of the spectra follows a different algorithm from that employed in a previous study of N_2 for the valence states by Khakoo *et al.* [Physical Review A **71**, 062703 (2005)], since the $^1\Pi_u$ and $^1\Sigma_u^+$ states form a strongly perturbatively-interacting valence-Rydberg series. The resulting data are compared to existing measurements.

PACS #s: 34.80.D, G, H; 33.15

1. Introduction.

Electron impact excitation of atomic and molecular targets plays a key role in a host of natural (aurorae, dayglow, interstellar emissions) and man-made environments (plasmas in lasers, etching plasmas, lighting discharges, etc). Considerable effort has been made in the past to both theoretically and experimentally determine electron scattering cross-sections for these targets. Whereas significant progress has been made for excitation of atomic targets, molecular targets remain difficult to model on account of their reduced symmetry and inclusion of rotational and vibrational degrees of nuclear motion, which couple into the electronic motion.

Recently, we carried out a careful and extensive series of energy loss measurements in molecular nitrogen covering the energy loss range of 6.25eV to 11.25eV from which we determined differential cross-sections (DCSs) for excitation of the $A^3\Sigma^+_u$, $B^3\Pi_g$, $W^3\Delta_u$, $B'\ ^3\Sigma_u^-$, $a'\ ^1\Sigma_u^-$, $a\ ^1\Pi_g$, $w\ ^1\Delta_u$ and $C\ ^3\Pi_u$ electronic levels from the $X\ ^1\Sigma_g^+$ ($v''=0$) ground state [1]. Whereas, significant disagreements were observed between our results and those of previous measurements and ours, a very recent *ab initio* theoretical study, by da Costa and Lima [2] using a perturbative multi-channel Schwinger method and Tashiro and Morokuma [3] using a close-coupling R-Matrix method, of these excitations showed significantly improved agreements between theory and experiments for the lower-lying states of N_2. We note here that best agreement was obtained between our earlier DCSs [1] and the close-coupling code [3]. On-going accurate time-of-flight measurements by Buckman and co-workers [4] is expected to shed more definitive light in this area. Recently, we have our N_2 measurements to examine excitation features in the energy loss range of 12eV to 13.8eV, which includes the quadrupole-allowed $a''^1\Sigma_g^+$ state and dipole-allowed $b\ ^1\Pi_u$, $c\ ^1\Pi_u$, $o\ ^1\Pi_u$, $b'\ ^1\Sigma_g^+$, $c_4'\ ^1\Sigma_u^+$, $F\ ^3\Pi_u$ and $G\ ^3\Pi_u$ states. The analysis of the energy loss spectra in these extended measurements differs from reference [1] in that perturbative (adiabatic) couplings between the Rydberg-valence and Rydberg-Rydberg $^1\Pi_u$ and the $^1\Sigma_u^+$ states [5] do not allow us to assume that the excitation cross sections of any electronic states′ vibrational levels are in proportion to Franck-Condon (FC) factors [2] as was done in reference [1]. The overall analysis of the spectral data thus followed a different algorithm than that used in reference [1], in that the spectra were fitted with all vibrational levels treated as independent transitions. We note that the exception here is the $a''^1\Sigma_g^+$ state, which, because of its different symmetry, should not affected by such perturbative interactions with nearby states. Therefore, its analysis is simplified in that the intensities of its vibrational level energy loss

features are found to remain largely in proportion with the FC factors for their excitation from the $X\,^1\Sigma_g^+$ (v″=0) ground state.

Electron excitation energy loss values (E) and dipole FC factors for excitation of the $X^1\Sigma_g^+$ (v”=0) to different v’ states are summarized in Table I, as obtained from different studies of the N_2 molecule. Past investigations of the electron impact excitation of the states of N_2 covered in this work are now summarized below. The reader is referred to the reviews of Itikawa et al. [12] and Itikawa [13], which cover research on e^-+N_2 up to 2005.

(i) The a” $^1\Sigma_g^+$ state: Lefevbre-Brion and Moser [14] from LCAO-MO-SCF calculations placed this state from excitation of the $X^1\Sigma_g^+ (1\sigma_g)^2 (1\sigma_u)^2 (2\sigma_g)^2 (2\sigma_u)^2 (1\pi_u)^4 (3\sigma_g)^2$ to the $(1\sigma_g)^2 (1\sigma_u)^2 (2\sigma_g)^2 (2\sigma_u)^2 (1\pi_u)^4 (3\sigma_g)^1 (3s+4p\sigma_g)^1$ i.e. one of the 3s electrons forming the $(3\sigma_g)^2$ molecular bond to a 4p orbital. This state can decay to the ground state only by quadrupole radiation, giving rise to the Dressler-Lutz system observed in high pressure plasmas. Electron impact excitation of this system was studied for only the $X^1\Sigma_g^+$ (v”=0) → a” $^1\Sigma_g^+$ (v’=0) by Lassettre et al. [17] at the high incident energy (E_0) of 500eV and small electron scattering angles (θ) to determine its generalized oscillator strength (GOS) as a function of momentum-transfer-squared (K^2), and showed that the GOS → 0 as K^2 → 0, typical of a forbidden transition. The first DCS measurements for the $X^1\Sigma_g^+$ (v”=0) → a” $^1\Sigma_g^+$ (v’=0,1) were measured by Cartwright et al. [18] and normalized to the then available elastic N_2 DCS standards. The DCSs were obtained at E_0= 15eV, 17eV, 20eV, 30eV and 50eV over the angular range of nominally 10° to 130° in 10° steps. These DCSs were then later renormalized to improved elastic N_2 DCS standards by Trajmar *et al.* [19]. It must be noted here that the results of this later renormalization obtained mixed results when compared with [1] for the excitation of the $A^3\Sigma^+_u$, $B^3\Pi_g$, $W^3\Delta_u$, $B'\,^3\Sigma_u^-$, $a'\,^1\Sigma_u^-$, a $^1\Pi_g$, w $^1\Delta_u$ and C $^3\Pi_u$ electronic transitions. In this work we will compare directly to [19]. This work was followed by similar measurements by Brunger and Teubner [20] using the best available elastic N_2 calibration standards, available to date. Their DCSs were obtained at E_0= 15eV, 17.5eV, 20eV, 30eV and 50eV over the nominal scattering angle (θ) range of 10° to 90° in 10° steps. Very good agreement with the DCSs of Cartwright et al. [18] was observed. At about the same time DCS ratios for the electron impact excitation of the $X^1\Sigma_g^+$ (v”=0) → a” $^1\Sigma_g^+$ (v’=0,1) relative to the $X^1\Sigma_g^+$ (v”=0) → {b $^1\Pi_u$(v’=0 to 7)+c $^1\Pi_u$(v’=0,1)+c’$^1\Sigma_u^+$ (v”=0,1)} were carried out by Furlan et al. [21]. This work was carried out at E_0= 35eV over the θ range of nominally -

30° to 80° in 10° steps Excellent agreement between these data and those of Trajmar *et al.* [19] (ratios were the same as Cartwright *et al.* [16]) was observed. Following this Zubek and King [22] made similar DCS measurements using the same elastic N_2 calibration standards as [19] and at E_0=17.5eV and 20eV over the angular range of 10° to 100° in 10° steps. Their DCSs showed some disagreement with those of Trajmar et al.[19] and Brunger and Teubner [20]. Also, a (small) dip in the DCSs at E_0>20eV, and θ of 20° was noted by Zubek and King and by Furlan *et al.*, but not investigated in any detail. The present work in this paper concerning DCSs for the electron impact excitation of the a" $^1\Sigma_g^+$ (v'=0,1) states has been reported by us elsewhere [23], and a fuller report is given here.

(ii) The excitation of the valence $b^1\Pi_u$ state of N_2 gives rise to the intense (b→X) UV Birge-Hopfield I bands and the (b→a) Gaydon-Herman near-UV bands. The Birge-Hopfield I bands have been investigated in detail by Carroll and Collins [24] and Dressler [25] in serial papers. A more recent study based on experimental observations using detailed perturbative analysis was done by Stahel et al. [7], and is the data used for comparison in this work as far as FC-factors and excitation energies is concerned (see Table 1). These bands reveal rich perturbative interactions between the $b^1\Pi_u$, $c^1\Pi_u$ and $o^1\Pi_u$ valence-Rydberg states. Differential electron scattering of the $b^1\Pi_u$, $c^1\Pi_u$ and $o^1\Pi_u$ valence-Rydberg states was carried out by Chutjian et al. [10], who unfolded the spectrum based on data in the form of excitation energies and FC factors, from reference [6, 24, 26 and 27]. However, since these FC factors are no longer constant with θ, due to perturbations, the method that was used (fixed FC factors) cannot be physically applicable here and to account for problems in fitting their spectra; this could be evidenced by the fact that they had to allow for several unknown states, M1, M2 and M3 to improve fits to their spectra. Even with this, their analysis of unfolding the spectrum was principally flawed and their results could not be expected to be correct. These DCS data were later corrected by Trajmar et al. [19], using a better elastic N_2 standard, but systematic problems regarding accounting of perturbations was still not taken care of in their correction.

Excitation of the Rydberg $c^1\Pi_u$ and $o^1\Pi_u$ levels give rise to the Worley-Jenkins UV bands and the Worley Rydberg series bands with decay to the ground state. Again perturbative interactions between $b^1\Pi_u$, $c^1\Pi_u$ and $o^1\Pi_u$ valence-Rydberg states causes these series to only be describable by adiabatic potentials. The DCSs for these states, from the work of Chutjian et al.

[10] (see above) did not account for perturbative interactions between the b, c. o $^1\Pi_u$ levels, but however, remain the only available DCSs to date for the upper levels of N_2.

(iv) Excitation of the b'$^1\Sigma_u^+$ and c'$^1\Sigma_u^+$ levels gives rise to the VUV Carroll-Collins-Yoshino and the Carroll-Yoshino bands. These states have significant mutual perturbations as observed by Dressler [25] and Carroll et al [28], which showed up as irregularities in vibrational and rotational structure. The b'$^1\Sigma_u^+$ state is predissociated at high v-levels, in particular the b'$^1\Sigma_u^+$ (v'=20, 20 and 22) $\rightarrow$ X$^1\Sigma_g^+$ (v'=0) bands showed clear diffusiveness in their rotational structure.

(v) Much work has been done on the spectroscopy of these levels and the reader is referred to the compilations in Lofthus and Krupenie [9] and Lefevbre-Brion and Fields [5]. Recently, a pre-dissociation study involving spin-orbit coupling between the b,c,o $^1\Pi_u$ and the C,C' $^3\Pi_u$ was carried out by Lewis et al [29], with the observation of heavy pre-dissociation of the b$^1\Pi_u$ state due to strong coupling between the b$^1\Pi_u$ and the C$^3\Pi_u$ in turn perturbed by the repulsive C' $^3\Pi_u$ continuum. Recently also, a theoretical investigation of the absorption spectrum of N_2 above the ionization threshold was made by Lefebvre-Brion [30] based on the laser work of McCormack et al. [28] to observe this region of the N_2 spectrum, excited from the a$^1\Pi_g$ (v=5) level. One of two towering absorptions were assigned by Lefevbre-Brion to the v"=44 of the b'$^1\Sigma_u^+$ state. Presently, the most recent tabulation of the energy levels of the b, c. o $^1\Pi_u$ levels and the b', c'$^1\Sigma_u^+$ levels remains the 1983 work of Stahel et al. [7], which is included in Table 1.

The present work is a first attempt to determine the DCSs for the b, c, o $^1\Pi_u$ states and the b', c'$^1\Sigma_u^+$ states of N_2, in the energy loss region of 12.0eV to 13.8eV using an analysis that accounts for the presence of perturbative interactions between these states, not dealt with in previous analyses. These DCSs also include attempts to correct the energry loss spectra for contributions from excitation of the D$^3\Sigma_u^+$, F$^3\Pi_u$ and G$^3\Pi_u$ (see Table 1) states, to obtain DCSs for these excitations also, in an attempt to complete the picture in this energy loss region.

2. Experimental:

II. Experimental Techniques and Procedures

Detailed descriptions of the apparatus are given in Khakoo *et al*. [32]. Briefly, cylindrical electrostatic optics and double hemispherical energy selectors were utilized both

in the electron gun and the detector. Energy loss spectra, including both the elastic peak and the inelastic region of interest, were collected at fixed impact energies and scattering angles by repetitive, multi-channel-scaling techniques. The target N_2 beam was formed by effusing the gas through a capillary array (with a collimation of 100) driven by a pressure of a few Torricelli behind it. The background signal was accurately determined using a moveable source method developed at CSUF [32]. The incident energy E_0 of the electron beam was determined by tuning the spectrometer analyzer to the elastic peak (energy loss: E=0) and then monitoring the energy loss spectrum to the maximum cut off in the energy loss spectrum (at $E=E_0$). The correct value of E_0 could be set by adjusting the appropriate electron gun bias power supply to obtain the required cut off voltage; this could be done to within 50meV. This provided for an easier method than the usual method of using the 2^2S resonance in the electron-helium scattering elastic channel, and gave excellent agreement with this method. The energy loss cut off method has the advantage, over the helium resonance method, that one does not have to change gases from N_2 to He, but it is however less precise.

The procedure for obtaining the normalized cross-sections consisted of several steps:

(i) In the first step, the spectrometer was tuned such that the elastic to inelastic ratios reproduced closely those from the TOF work of LeClair and Trajmar [34] which are accurate on a relative scale to ±5%. The analyzer was baked and maintained in a very clean vacuum environment so that this response remained stable. At low residual energy E_R ($=E_0-E$), by using the helium ionization continuum at E_0=30eV (which has been shown to be flat within 5%; see Schow et al. [35]) the transmission could be closely (within 10%) described by the function (see also Khakoo et al. [1]) :

$$T(E_R) = 0.055 \ln(E_R) + 0.87. \qquad (1)$$

This function was applied to the spectrum obtained at E_0=17.5eVonly, since these were the spectra affected outside of error bars at E_R<4eV.

(ii) We now accumulated energy loss spectra in the energy loss range of 12eV to 14.5eV, and unfolded these in the energy loss range of 12.0eV to 13.82eV leaving all vibrational levels in Table 1 as independent features. Hence, the multi-channel spectrum

$$S_i(E_0,\theta,E_i) = C\sum_{nv'}\boldsymbol{\sigma}_{nv'}(E_0,\theta)\ F(E_i - E_{n,v'}) + \mathbf{B}(E_0,\theta,E_i,\rho,I_0) \qquad -(2)$$

was fitted to all features appertaining to the nth electronic state with its v'^{th} vibrational level at the energy loss for the ith channel or bin, except that in this case the normalized instrumental line function,

$$F(E - E_{n',v'}) = \sum_{m=1}^{M} \frac{A_m}{\Delta_m \sqrt{\pi}} \exp\left[-\left[\frac{E - E_{n',v'} - E_m}{\Delta_m} \right]^2 \right] \qquad -(3)$$

is a multi-Gaussian function (with M possible up to 5 and, with each Gaussian located off the line center by the energy loss amount E_m, relative intensity A_m and, having the width Δ_m. Note: In this work, we used M values that were ≤ 2). Here, $E_{n,\,v'}$ is the energy loss value for the v' vibrational level of the n' electronic state (see Table 1). The function F in equation 3, was synthesized from a non-linear least-squares fitting to an isolated feature (usually the $a''^1\Sigma_g^+$ (v'=0 feature). The fitting yields a relative DCS C $\sigma_{nv'}$ where C is a constant for each spectrum that must be determined by normalization of the spectrum to an absolute DCS standard. (see later). Transition energies for the X(v''=0)→ b, c, o, b' and c' optically allowed features and the D, G, F optically forbidden features in the energy loss region of interest were taken from a semi-empirical investigation by one of us and for the a'' features, were taken from a best fit to the experimental data at small θ.. The function

$$B(E_0, \theta, E_i, \rho, I_0), = \sum_{k=0}^{K<3} \mathbf{B_k} E_i^k \qquad -(4)$$

which represented the background was expressed as a polynomial of up to order 2 and was dependent on the incident electron current I_0 and target gas density distribution ρ. In equation 2 and 4 the variables $C\sigma_{nv'}(E_0, \theta)$ and B_i were determined by linear least squares fitting to the spectrum (Note: The $\sigma_{nv'}(\varepsilon_0, \theta)$ will later be determined from the relative $C\sigma_{nv'}(\varepsilon_0, \theta)$ values upon normalization to a known cross-section). By summing up the intensities of all features in the energy loss spectrum it was possible to determine the fractional intensity of the feature nv' of the whole spectrum. Two further features to improve the fits to the spectrum were:

(a) That the function in equation 2 could be varied non-linearly in E, to further minimize the residual of the fit, i.e. energy loss at the start of the spectrum E_1 (see was changed in successively reduced increments until a minimum in the reduced chi–squared value (χ^2_ν)

was reached. Importantly it was observed that the resultant minimum in χ^2_ν was (uniquely) global for the spectrum.

(b) The step size, δE (= energy loss per unit bin), was varied in very small amounts, in corroboration with (a), to minimize χ^2_ν. The linearity in the computer ramp voltage (provided by a 0-10V 12-bit D-A converter) to the power-supplies that control the analyzer (detector) side of the spectrometer, and therefore determines the energy loss value, was typically ±2mV in a 5V span. However, the improvements in χ^2_ν that were observed when doing this secondary correction were significantly smaller than in (a), and typically a factor of less than 0.1 of the changes in (a). This is because δE did not vary significantly during the course of the experiment.

Steps (a) and (b) resulted in improved fits as gauged from values (χ^2_ν) which were typically in the range of 1-3 for typically 800 data points with ~53 variables (i.e. the number of degrees-of-freedom, $\nu \approx 747$). Typical unfolded spectra are shown in Figure 1. The spectrometer was found to be very stable, yielding currents of about 7-10nA with an energy resolution of 30-35meV (FWHM).

However several energy loss lines overlapped within 10meV and could not be separated by the resolution of our spectrometer (see Table 1), i.e. b(4) and D(0), b(5) and F(0), o(0) and D(1), c(1) and F(1), o(1) and b(9), b'(6) and G(2), b'(8) and o(2). In this case the fitting routine (using a singular-value decomposition routine) set one of the pairs' intensities to zero. Increasing the resolution of the spectrometer would have required a reduction of the electron current and consequently a reduction in the scattered electron signal, and a resulting worsening of statistical error incurred in the data. The present setup is therefore a compromise to obtain as broad a coverage of the line intensities as a function of scattering signal as could be reasonably possible in a practical amount of time (in this case it took us 8 months of essentially continuous running time to obtain the data presented here.

(iii) At this point the method described by Nickel *et al*. [36] using the elastic electron-N_2 DCSs was carried out to place our total spectral intensities on an absolute DCS scale as follows:

(a) Firstly using the moveable source method (Hughes *et al*. [33]) we simultaneously measured the elastic spectrum (-.25eV to +0.25eV energy loss) and inelastic energy loss

spectrum (6eV to 14.5eV energy loss) with the gas source aligned into the electron beam (Signal + Background; IN) and then moved out of alignment (Background; OUT). The subtracted result of the OUT spectrum from the IN spectrum could be used to determine the relative DCS of the summed A+W+B+B'+a'+a+w+C states (region-1; E from 6eV to 11.5eV) and a", b+c+o+b'+c'+D+F+G (region-2; E from 12eV to 13.8eV). Note, the spectrum was determined with lowered statistics that of the spectra in (ii), i.e. a fewer number of channels were used and also fewer scans, since we did not need to unfold such spectra. However, the summed statistical uncertainty was always better than 3% on average after subtraction of the background.

(b) Relative DCSs were then obtained by normalizing the elastic peak counts to an average of selected experimental DCSs for elastic electron scattering from N_2 of Srivastava *et al*. [37], Shyn and Carignan [38], (renormalized by Trajmar *et al*. [19]), Nickel *et al*. [39] and Gote and Ehrhardt [40] . These data are tabulated in Trajmar *et al*. [19] and Brunger and Buckman [41]. In our selection, we used those values of elastic scattering DCSs for which the measurements showed agreement with each other within error bars.

(c) We renormalized the summed DCS data, obtained in (iii.a), using the inelastic to elastic DCS ratios obtained from the TOF measurements of LeClair and Trajmar [34] at $\theta=90^o$, which should be very reliable and have an uncertainty of <10%. We further compared the inelastic to inelastic ratios for the regions 1 to our earlier measurements [1]. These normalized inelastic to elastic ratios are listed in Table 2 in addition to a third region from 12eV to 14.5eV at $\theta=60^o$, 90° and 120°. These (estimated) uncertainties are also incorporated into our data because of the systematic uncertainty in applying a correction at near-threshold to the energy loss spectra.

The experimental error, assigned to the various quantities, is the square root of the sum of the squares of the contributing error components. For the DCS values associated with the sum of the nine state excitations at 90°, we considered the statistical and fitting errors in the individual scattering intensities (typically 2% to 25%) and the inelastic/elastic ratio error of the TOF results of LeClair and Trajmar [34] (≈10%), the error on the available elastic scattering DCSs (≈14%), the error propagated by the inelastic to elastic ratio measurements (typically 5%) and an additional error of 10% for the analyzer response function. We also importantly note here that no smoothing is applied to the final shape of our DCS data. Our

DCSs and associated uncertainties are listed in Tables 3a to 3e. These DCSs are graphically compared to existing measurements and theoretical values in Figures 2 to 8.

III. Additional Details

The present direct unfolding of the energy spectrum yielded measurements of DCSs for the excitation of partial b-state (b=b(0)+…b(13)+D(0)+F(0)), partial c-state (c=c(0)+...c(3)+F(1)), partial o-state (o=o(0)+…o(3)+b'(8)), partial b'-state (b'=b'(0)+..b'(10)+G(2) not including b'(8)+o(2)) and c'-state (c'=c'(0)+..c'(3)). The only forbidden transitions that could be completely resolved were G(0), G(1), D(2), D(3), G(3) and F(3). The FC factors for these levels (see Table 1) were computed from RKR calculations using an RKR code from Gilmore et al. [40] using the molecular constants for these levels listed in Lofthus and Krupenie [9]. Incidentally, the paper of Gilmore et al. [40] also has very useful spectroscopic data for various low-lying bands of N_2, covered in previous work [1,40] in our groups. Using the intensities for the resolved G, D and F states we corrected the b, c, o and b', c' for contributions from these states, assuming that the F and G do not interact perturbatively and are therefore diabatic. From the intensity ratios of the resolved G, D and F (v) levels, we determined semi-empirical FC-factors, using the theoretical FC-factors to interpolate for the unresolved G, D and F (v) levels. Since these we can also use the data to interpolate (by regression) our experimentally resolved level FC-factors to those of the unresolved levels. As a result, our final DCSs are for the b(=b(0)+…b(13)), c-state (=c(0)+...c(3)), o-state (o=o(0)+…o(3)+b'(8)), partial b'-state (b'=b'(0)+..b'(10)) not including b'(8)+o(2)) and c'-state (c'=c'(0)+..c'(3)). The only forbidden transitions that could be completely resolved were G(0), G(1), D(2), D(3), G(3) and F(3), and these were used to extricate full state DCSs for the G, D and F states.

In addition, the statistical errors of the individual weak nv' lines, are large, and in this study we have a few selected representative dominant nv' lines of different electronic states in an effort to show differences in the shape of their DCSs as a function of θ, at different E_0 values, thus to demonstrate large variations in their "FC-factors" as a function of θ, at different E_0 values.

IV. Results and Discussion.

Tables 3(a-e) display the DCSs for the electron impact excitation of the transitions measured in this work. The average errors are also given in these tables. Unfortunately, the intensities of the D(2) and D(3) levels were mostly very small and could not be used to interpolate the DCSs for the D state. Consequently, this excitation is not measurable in our experiment. We now address the DCSs for the individual excitations. In later comparison with the earlier work of Trajmar et al. [19], we find this result is similar to that observed by Chutjian et al. [10]/Trajmar et al. [19], i.e. they also did not observe any significant scattering intensity for the D $^3\Sigma_u^+$ state excitation.

(1) a'' $^1\Sigma_g^+$ excitation. Figure 2(a) to (e) show our DCSs for excitation of the X $^1\Sigma_g^+$ (v"=0) → a''$^1\Sigma_g^+$ (v'=0,1). The results are compared to earlier measurements. From Figure 2a (E_0=17.5eV), we observe that our DCSs are a factor of 2 lower than those of past measurements, i.e. in Trajmar et al. [19] (at E_0=17eV), Brunger and Teubner [20] (at E_0=17.5eV) and Zubek and King [22] (at E_0=17.5eV). Our DCSs show a sharp drop at $\theta<8^o$ which is not unexpected for a forbidden Σ↔Σ transition. In addition the shape of our DCSs at $\theta>80^o$ is in marked difference from the other values. We also note at $\theta=30^o$, a small inflection in the DCS trend. This quantitative difference in the earlier measurements is likely due to transmission of the instruments, however we also note that our DCSs have the advantage of being corrected by the TOF results of [34], and are probably systematically closer to the correct values. In Figure 2(b), (E_0=20eV) the disagreement factor of 2 still remains, but the DCS shapes at $\theta>80^o$ show improved agreement with the earlier work. We note that because of the coarser angular steps used in the earlier measurements, they overstep the developed cusp in the a" DCS at $\theta=25^o$. In Figure 2c, (E_0=30eV) the quantitative agreement shows improvement with Trajmar et al.'s [18] DCSs, except for their downward trend in DCSs which opposes their trend at the lower E_0 value of 20eV. Qualitative agreement with Brunger and Teubner's [20] DCSs is better, but they are higher than ours by a factor of about a half. We note the developed cusp in the a" DCSs observed in this work. At E_0=50eV (Figure 2d) agreement between the DCS measurements is very good, again with the DCSs of [19] showing the rise at larger $\theta>110^o$. In fact we observe a steep rise in the DCSs by over a factor of 4 from the DCSs of [19]. At this E_0 value, both measurements observe the effect of the cusp, but do not probe it because of the coarser angular spacing of their work. The cusp is

clearly observed here at $\theta=20^o$ with an angular width of about 9°. At E_0=100eV (Figure 2e), this cusp still persists.

This cusp is interesting because it is likely due to channel-coupling effects, similar to cusps observed in atomic transitions with the same symmetry for the lower and upper states, e.g. the 1^1S to 2^1S transition in He, and has been discussed in detail in an earlier paper by our group [41]. It is probably not as pronounced in molecules as it is atoms, on account of being washed out by alignment and rotational effects in the molecule, not present in atoms. It would be of interest for a theoretical investigation to look at this transition in the fixed-nuclei approximation to see how pronounced this cusp is, and adding rotation to see how rotation may affect the depth of this feature. This is the first time to our knowledge that such a cusp, in differential scattering, has been observed.

The disagreement between our DCSs and those of Brunger and Teubner [20] for this transition may also explain the disagreements between our DCSs for the lower transitions in N_2 published in [1], since they used the scattering intensity of the $a''^1\Sigma_g^+$ state as a calibration check in their electron scattering measurements (see [20]). In this case the DCS cusp in this excitation does not affect the overall total excitation cross-section determinations (from the DCSs) by more than 15% (see e.g. [43]), but it will significantly affect the angular distributions of these measurements in the region of around 20°.

We also note here that from our measurements, that the $a''^1\Sigma_g^+$ state v"=0 dominates this excitation, taking ≈ 85% of the FC-factor. Interestingly, at large scattering angles ($\theta > 70^o$), the $a''^1\Sigma_g^+$ (v'=1) feature becomes broadened, best corrected by adding a state at the energy loss value of 12.540eV (see "M" in Table 1). If M is not included at large angles, the FC-factors linearly averaged over angles gives a value of 0.89 and 0.11 for the $a''^1\Sigma_g^+$ state v"=0 and 1, respectively. The contribution from the M-feature is included in the DCSS for the $a''^1\Sigma_g^+$ state. The broadening is not presently understood.

(2) Excitation Differential Cross-sections.

(a) b, c, o $^1\Pi_u$ state excitations. Figures 3 and 4 show the DCSs for excitation of the b, c, o $^1\Pi_u$ states in the energy loss window of this work, i.e. for the summed v" above the middle line in Table 1 at representative E_0 values of (3a,4a) 20eV and (3b, 4b) 50eV. From these figures, it is evident that all three excitations show similar angular pattern with a rapid change

in the region of θ around 40°-60° at E_0=20eV. However, some (small) differences at larger scattering angles can be observed, especially for the $o^1\Pi_u$ excitation. At E_0=50eV (Figures 3b, 4b) these differences are almost negligible, and typical of Rydberg states of the same symmetry. As expected all show clear forward scattering patterns typical of dipole-allowed transitions.

At 50eV (Figure 4a, 4b) we compare with the DCSs of Trajmar [19] for these excitations. The DCSs of Trajmar et al. [19] were taken at E_0=40eV and 60eV. So for this comparison, an average of the two data sets was taken. The agreement between the two data sets is surprisingly remarkable, considering that the earlier measurements used an FC-factors algorithm to unfold their spectrum. The FC factors were obtained from [6, 24, 26 and 27] the problems in fitting an FC-factor-based algorithm to the spectra (due to the effect of significant perturbative interactions in the N_2 spectrum somewhat forced Chutjian et al. [10] to add levels M1, M2 and M3 in their spectral fitting. Also, it is not clear how they would have prevented a distorted fit of their spectra especially for the strong perturbations between the b-c states around b(v”=5,6 and 7) and c(v”=0,1). We have allowed estimated error bars from their data base on their figures of about 40%. Nevetheless, agreement between the present DCSs and those of Trajmar et al [19], for the b and c states is excellent. In the energy loss range of this work, we capture (based on dipole FC factors from Stahel et al. [8]) 97.7% of the intensity for the b state, 100% of the c-state intensity and 92.4% of the o-state intensity. With this result we note that the significant disagreement for the c-state DCSs between our DCSs and Chutjian et al./Trajmar et al. [10,19] is not clear. It could be due to large perturbative effects in the spectra, at the higher energy loss values, which could not be fitted by the FC-factors' method used by [10,19]. Overall, however, the agreement is very encouraging and probably indicates that a theoretical method that does not explicitly deal in the perturbative effects, could probably give reasonable results.

(b) b', c' $^1\Sigma_u^+$ state excitations. Figures 5 and 6, show the DCSs of the b' and c' states at E_0 values of 20eV and 50eV. We observe similar results as we did for the b, c and o states at these energies. Some variation in angular behavior can be seen at large θ values, but on average these DCSs show clear Rydberg behavior for these states. Comparison with the DCSs of Trajmar et al. [19] is excellent especially for the c' state, where remarkably close agreement in the shapes of the two data sets across the whole angular range is observed. In the

energy loss range of this work, similarly as for the b, c and o states, we capture (based on dipole FC factors from Stahel et al. [7]) 8.48% of the intensity for the b' state, and 84.74% of the c'-state intensity. Much of the b' state intensity lies outside of the present work's energy loss range. In the measurements of Trajmar et al. [19], with energy loss extending to 14.2eV, 40% of the b' state spectrum was captured. Hence, the very good agreement between the two data sets is very surprising at present.

(c) G, F $^3\Pi_u$ excitations. In Figures 7 and 8, we show representative DCSs for these excitations at E_0=17.5eV and 50eV. At 17.5eV, these excitations display DCSs that are typical of forbidden excitations and angular distributions that are similar, thus typifying their Rydberg nature. At large θ, the F state DCSs show a different angular behavior, indicating that these states may be coupled differently to neighboring states. At E_0=50eV, comparison with the DCSs of Trajmar et al [19] is good at forward angles, but marked deviations between our results and theirs at $\theta>80^o$ are observed. Whereas both sets of DCSs show an upturn, those of Trajmar et al. [19] are considerably larger than ours. We note that in this case we are considering 100% of the G and F states in our analysis, since almost all of their intensity lies in the energy loss range of the present work.

(3) Excitation Optical Oscillator Strengths.

The present DCSs for the optically allowed transitions, at E_0=100eV, were converted to apparent oscillator strengths (AGOS). These are apparent GOS because the Born approximation may not be valid at this value of E_0. The AGOS is given by:

$$\mathrm{AGOS}(K^2) = \frac{E}{2} K^2 \sqrt{\frac{E_0}{E_n}} \ \mathrm{DCS} \qquad (5)$$

, where K^2 (the momentum transfer squared), E, E_0 and E_n =(E_0-E) and the DCSs are in a.u. These AGOSs were then extrapolated to $K^2 \rightarrow 0$ to the Apparent Oscillator Strengths (AOOS) using the (well-established) polynomial extrapolation method developed by Vriens [44], and then the extrapolation scaled up by the fraction of the sum of optical FC-factors covered in our spectrum range. So for example, the b state was multiplied by 1/0.9664. The results of this are given in Table 4. These results are compared to the OOS for the various states from the work of Trajmar et al. [19], the diabatic and adiabatic transition moments and Optical Oscillator Strengths (OOS) values from Stahel et al. [7]. The (absorption) OOS of Stahel et al. were computed from the formula

$$OOS = \frac{2}{3}\frac{g_j}{g_i}|M_{ij}|^2 \quad E \qquad (6)$$

, for a transition for a lower state i and upper state j with statistical weights (2S+1)*(g_Λ), g_Λ being 2 for Π states and 1 for Σ states. Thus for the $^1\Sigma \rightarrow {}^1\Sigma$ transitions, $g_i/g_j = 1$ and for the $^1\Sigma \rightarrow {}^1\Pi$ transitions, $g_i/g_j = 2$. $|Mij|^2$ are squared transition moments. Since both OOS and transition moments $|Mij|^2$ are presented in {7], we can compute their mean E values or centroid energies using equation 6. The centroid energies from our present are obtained in the region of energy loss from 12.0eV to 13.82eV, and are a weighted average of our excitation energies - weighted by the FC factors (optical spectra at $\theta<3^o$; see Section III). These energies show reasonable agreements with those of [9]. The OOS [9] for the adiabatic work of Stahel et al. [7] are in significantly better agreement with ours than their diabatic OOS values. All our AGOS values are reasonably placed when compared to those of [7], except for the b' state, where the correction factor (=1/0.0848) is a large correction to the b' AOOS, and will very likely not be a reliable value. It is also most probable that it is our significant value of the b' AOOS which upsets our summed AOOS from coming near to the value of 0.6 from 0.7 as observed by Chutjian et al. [10] and Lassettre in [10] (AGOS L). For the c' $^1\Sigma_u^+$ OOS values, our value of 0.081 ± 0.023 is too small when compared to the experimental values around 0.14 with errors around the 20% area.

V. Conclusions.

Using a high-resolution electron spectrometer as well as accurate (deperturbed) energy levels for the vibrational levels of the N_2 molecule in the 12.0 to 13.82 eV excitation energy loss range, we have been able to unfold much of the spectra of the molecule and obtain improved DCSs for excitation of these levels. The present work is the first attempt to obtain DCSs for excitation of the Rydberg-valence states from the ground state at a large range of E_0 values, and closely space θ intervals including fro the effect of perturbations, which was not done in the earlier work of Trajmar et al. [10,19] which was also done at two very closely place E_0 values of 40eV and 50eV. The results were unexpectedly surprising:

(a) The present DCSs at the E_0 values of 50eV compared (surprisingly) excellently with those of [10,19] which were taken from the averaged DCSs of their E_0=50eV and E_0=60eV data

sets. This perhaps suggests some sort of a sum rule between the excitation of a state that even if perturbed, still retains an overall intensity. However, we do not understand how biasing the spectral fits with optical FC-factors (as was done in [10, 19]) would yield DCSs close to ours.

(b) Similar to the observations of Trajmar et al. [10,19] we were not able to observe any significant intensity in the excitation of the D metastable state. This was also an interesting observation after we had analyzed our data, and compared with Trajmar et al. [19].

(c) Significant perturbative deviations from fixed FC-factors was observed in the b-c systems. This observation will be the subject of a future paper.

(d) A very interesting cusp was observed for the DCS of the a" state at θ around 20°. This cusp begins at E_0 around 20eV and persists to 100eV. This is the first excitation cusp observed for molecules and we hypothesize that it is a result of channel-coupling since the ground X and a" have the same $^1\Sigma_g^+$ symmetry. A close-coupling calculation would reveal such an effect.

VI. Acknowledgements: The work carried out at California State University, Fullerton was funded by the National Science Foundation under grant # NSF-PHY-RUI-0096808. The research carried out at the Jet Propulsion Laboratory (JPL), California Institute of Technology was sponsored by the National Aeronautics and Space Administration. Financial support through NASA's Planetary Atmospheres program is gratefully acknowledged. This research was performed while CPM held a National Research Council Research Associateship award at JPL. Valuable communications with Dr. K. Bartschat (Drake U., Iowa) regarding channel-coupling effects are gratefully acknowledged.

Table Captions:

Table 1. Energy loss positions in eV (left) and normalized Franck-Condon factors (right) for the excitation of the $a''^1\Sigma_g^+$, b $^1\Pi_u$, c $^1\Pi_u$, o$^1\Pi_u$, b′ $^1\Sigma_g^+$, c_4' $^1\Sigma_u^+$, D $^3\Sigma_u^+$, F $^3\Pi_u$ and G $^3\Pi_u$ (v") levels from the $X^1\Sigma_g^+$ (v'=0) ground state. References: P, Present work, limited to E of 13.82eV and with the E values used in the unfolding of present spectra; GS, Geiger and Schröder [6]; SLD., Stahel, Leoni and Dressler [7]; H., Hammond *et al.* [8]; LK, Lofthus and Krupenie [9], either directly from tables or from RKR calculations using their molecular constants for the electronic levels; CCT1, from Chutjian et al. [10] and CCT-2 from Trajmar [11]. The present dipole-FC-factors for the dipole allowed states are an average taken from unfolding electron energy loss spectra obtained at E_0=30eV, 50eV and 100eV for $\theta \leq 3^o$. Our FC factors are corrected by taking into consideration the remaining intensity of the electronic state using the FC data from Stahel et al. [7], outside of our experimental region of 13.82eV. For the b, c, o, b' and c' state, this meant multiplication by the factors of 0.977, 1, 0.924, 0.0847 and 0.847, respectively. For the forbidden G, D and F excitations, the FC-factors are determined from a combination of present experimental intensities and RKR calculations (see Section III). Present E values were obtained from a present semi-empirical study by one of us (B. R. Lewis). Italicized data correspond to grouping of levels that are not resolvable by our spectrometer. See text for additional discussion.

Table 2. Elastic to inelastic ratios for electron scattering from N_2, using the moveable source method [31]. The elastic DCSs used were the same as those used in our earlier work [1], and can be computed from the table. The inelastic ratio spans the energy loss window of 12.0eV up to 13.82eV covering the range of levels given in Table 1.

Tables 3(a-e). Differential cross-sections for the electron impact excitation of the X $^1\Sigma_g^+$ (v″ = 0) → $a''^1\Sigma_g^+$, the b$^1\Pi_u$, c$^1\Pi_u$, o$^1\Pi_u$, b′ $^1\Sigma_u^+$ and c′ $^1\Sigma_u^+$ and the F $^3\Pi_u$ and G $^3\Pi_u$ transitions in N_2 at different E_0 values. (a) E_0 = 17.5eV, (b) E_0 = 20eV, (a) E_0 = 20eV, (d) E_0 = 50eV and (e) E_0 = 100eV. Error bars include errors on the elastic electron scattering DCS (14%), elastic to inelastic transmission errors (5-10%) and statistical/unfolding errors (10-25%). The average error is given at the bottom of each column.

Table 4. Apparent Optical Oscillator Strengths (AOOS) and Optical Oscillator Strengths (OOS) values for the electron impact excitation of the $X\,^1\Sigma_g^+ (v'' = 0) \rightarrow a''\,^1\Sigma_g^+$, the $b^1\Pi_u$, $c^1\Pi_u$, $o^1\Pi_u$, $b'\,^1\Sigma_u^+$ and $c'\,^1\Sigma_u^+$ transitions in N_2. These values (P) were taken at E_0=100eV using DCSs at θ<20°. See text for details regarding centroid energies of the excitation spectra. References are indicated where this work was published. AOOS L is the work of Lassettre published in [10] as a private communication. Our correction factor (labeled Correction Factor in the table) for our AGOS values is a simple sum of the ratio of the state FC-factors for the E range of 12.0eV to 13.82eV (see Table 1) compared to the full sum using the FC factors in [7]. The present partial AOOS values must be divided by this correction factor to obtain the corrected AOOS values, which should be a better estimate of the full state AOOS.

Figure Captions.

Figure 1: Electron energy loss spectra of N_2 taken at E_0=50eV and scattering angles of (a) 3° and (b) 20°. The positions of the various spectral lines, except the triplet valence-Rydberg states, are indicated on the figures. These angles are chosen to highlight the significant relative decrease of the height of the a″ $^1\Sigma_g^+$ (v′=0) state energy loss feature (located at 12.255eV energy loss, in (b), at the DCS minimum) and, also to highlight the significant rise in the $b^1\Pi_u$ (v'=6) feature as compared to (a). The dots are the present experimental data and the line is a spectral fit using energy loss data from Table I, present work P.

Figure 2. DCSs for the electron impact excitations of the a″ $^1\Sigma_g^+$ state at (a) 17.5eV, (b) 20eV, (c) 30eV, (d) 40eV and (e) 100eV. Legend: • Present work; □ Trajmar *et al*. [19] (at E_0=17eV); × Brunger and Teubner [20]; o Zubek and King [22].

Figure 3. DCSs for the electron impact excitations of the $b^1\Pi_u$, $c^1\Pi_u$ and $o^1\Pi_u$ states at E_0 =17.5eV. Legend: • Present work. DCS units are in $10^{-18}cm^2/sr$.

Figure 4. DCSs for the electron impact excitations of the $b^1\Pi_u$, $c^1\Pi_u$ and $o^1\Pi_u$ states at E_0 = 50eV. Legend: • Present work; □ Trajmar *et al*. [10,19] average of their E_0=40eV and 50eV DCSs. DCS units are in $10^{-18}cm^2/sr$.

Figure 5. DCSs for the electron impact excitations of the b′ $^1\Sigma_u^+$ and c′ $^1\Sigma_u^+$ states at E_0 = 17.5eV. Legend: • Present work. DCS units are in $10^{-18}cm^2/sr$.

Figure 6. DCSs for the electron impact excitations of the b′ $^1\Sigma_u^+$ and c′ $^1\Sigma_u^+$ states at E_0=50eV. Legend: • Present work; □ Trajmar *et al*. [10,19] average of their E_0=40eV and 50eV DCSs. DCS units are in $10^{-18}cm^2/sr$.

Figure 7. DCSs for the electron impact excitations of the $G^3\Pi_u$ and F $^3\Pi_u$ states at E_0 = 17.5eV. Legend: • Present work. DCS units are in $10^{-18}cm^2/sr$.

Figure 8. DCSs for the electron impact excitations of the $G^3\Pi_u$ and $F\ ^3\Pi_u$ states at E_0=50eV. Legend: • Present work; □ Trajmar *et al*. [10,19] average of their E_0=40eV and 50eV DCSs. DCS units are in $10^{-18}cm^2/sr$.

References:

(1) M. A. Khakoo, P. V. Johnson, I. Ozkay, P. Yan, S. Trajmar and I. Kanik, Phys. Rev. A **71**, 062703 (2005).

(2) R. F. da Costa and M. A. P. Lima, International J. Quantum Chem. **106**, 2664 (2006).

(3) M. Tashiro and K. Morokuma, Phys. Rev. A **75**, 012720 (2007).

(4) S. F. Buckman, Gaseous Electronics Conference, Ohio State University, *Near-Threshold Electron Impact Excitation of the Electronic states of N_2*, LW2.00006, 2006.

(5) H. Lefebvre-Brion and R. W. Field, *The Spectra and Dynamics of Diatomic Molecules*, Elsevier, San Diego, 2004.

(6) J. Geiger and B. Schröder, J. Chem. Phys. **50**, 7 (1969).

(7) D. Stahel, M. Leoni and K. Dressler, **79**, 2541 (1983).

(8) P. Hammond, G. C. King, J. Jureta and F. H. Read, J. Phys. B: At. Mol. Opt. Phys. **20**, 4255 (1987).

(9) A. Lofthus and P. H. Krupenie, J. Phys. Chem. Ref. Data, **6**, 113 (1977).

(10) A. Chutjian, D. C. Cartwright and S. Trajmar, Phys. Rev. **A16**, 1052 (1977).

(11) S. Trajmar, Private Communication, 1995.

(12) Y. Itikawa, M. Hayashi, A. Ichimura, K. Onda, K. Sakimoto, K. Takayanagi, M. Nakamura, H. Nishimura and T. Takayanagi, J. Phys. Chem. Ref. Data, **15**, 985 (1986).

(13) Y. Itikawa, J. Phys. Chem. Ref. Data, **35**, 31 (2006).

(14) H. Lefebvre-Brion and C. M. Moser, J. Chem. Phys. **43**, 1394 (1965).

(17) E. N. Lassettre, A. Skerbela and V. D. Meyer, J. Chem. Phys. **65**, 3214 (1966).

(18) D. C. Cartwright, S. Trajmar, A. Chutjian and W. Williams, Phys. Rev. A **16**, 1031 (1977).

(19) S. Trajmar, D. F. Register and A. Chutjian, Phys. Reports **97**, 219 (1983).

(20) M. J. Brunger and P. J. O. Teubner, Phys. Rev. A **41**, 1413 (1990).

(21) M. Furlan, M-J. Hubin-Franskin, J. Delwiche and J. E. Collin, J. Phys. B: At. Mol. Opt. Phys. **23**, 3023 (1990).

(22) M. Zubek and G. C. King, J. Phys. B: At. Mol. Opt. Phys. **27**, 2613 (1994).

(23) M. A. Khakoo, R. Laher, S. Wang, R. Laher, P. V. Johnson, C. P. Malone, and I. Kanik, . Phys. B: At. Mol. Opt. Phys., in press (2007).

(24) P. K. Carroll and C. P. Collins, Canad. J. Phys. **47**, 562 (1969).

(25) K. Dressler, Canad. J. Phys. **47**, 547 (1969).

(26) G. Joyez, R. I. Hall, J. Reinhardt and J. Mazeau, J. Elect. Spectry. Rel. Phen., **2**, 183 (1973).

(27) D. C. Cartwright, Phys. Rev. **A2**, 1331 (1970).

(28) P. K. Carroll, C. P. Collins and K. Yoshino, J. Phys. B **3**, L127 (1970).

(29) B. R. Lewis, S. T. Gibson, W. Zhang, H. Lefebvre-Brion and J-M Robbe, J. Chem. Phys. **122**, 144302 (2005).

(30) H. Lefebvre-Brion, J. Chem. Phys. **122**, 144315 (2005).

(31) E. F. McCormack, S. T. Pratt, J. L. Dehmer and P. M. Dehmer, Phys. Rev. A **42**, 5445 (1990).

(32). M. A. Khakoo, C. E. Beckmann, S. Trajmar and G. Csanak, J. Phys. B: At. Mol. Opt. Phys. **27,** 3159 (1994).

(33) M. Hughes, K. E. James , J. G. Childers and M. A. Khakoo, Meas. Sci. Technol. **14**, 841 (2003).

(34). L. R. LeClair and S. Trajmar, J. Phys. B: At. Mol. Opt. Phys. **29**, 5543 (1996).

(35). E. Schow, K. Hazlett, C. Medina, G. Vitug, J. Childers, I. Bray and M. A. Khakoo, Phys. Rev. A **72**, 062717 (2005).

(36) J. C. Nickel, P. W. Zetner, G. Shen and S. Trajmar, J. Phys E **22**, 730 (1989).

(37) S. K. Srivastava, A. Chutjian and S Trajmar, J. Chem. Phys. **64**, 1340 (1976) corrected in reference [18].

(38). T. W. Shyn and G. R. Carignan, Phys . Rev. A **22**, 923 (1980).

(39). J. C. Nickel, C. Mott, I. Kanik, D. C. McCollum, J. Phys. B: Atom. Mol. Phys. **21**, 1867 (1988).

(40). M. Gote and H. Ehrhardt, J. Phys. B: Atom. Mol. Opt. Phys. **28**, 3957 (1995).

(41). M. .J. Brunger and S. J. Buckman, Phys. Rep. **357**, 215 (2002).

(42). F. R. Gilmore, R. R. Laher and P. J. Espy, J. Phys. and Chem. Ref. Data, **21**, 1005 (1992).

(43) P. V. Johnson, C. P. Malone, and I. Kanik, K. Tran and M. A. Khakoo, J. Geophys. Res. **110**, A11311 (2005).

(44) L. Vriens, Phys. Rev. **160**, 100 (1967).

(45) G. M. Lawrence, D. L. Mickey and K. Dressler, J. Chem. Phys. **48**, 1989 (1968).

(46) G. Stark, K. P. Humer, K. Yoshino, M.–C. Chan, T. Matsui, P. L. Smith and K. Ito, Astrophys. J. **531**, 321 (2000).

(47) J. Ajello, G. K. James, B. O. Franklin and D. E. Shemansky, Phys. Rev. A **40**, 3524 (1989).

	Excitation Energies (eV)							Franck-Condon Factors			
Level	P	GS	SLD	H	LK	CCT-1	CCT-2	CCT-2	SLD	P	Error
a"(0)	12.255			12.255			12.253	0.870		0.848	0.031
b(0)	12.4997	12.500	12.500	12.500	12.4996	12.533	12.500	0.010	0.0105	0.014	0.001
a"(1)	12.516			12.520			12.516	0.130		0.152	0.022
M ?	12.540										
b(1)	12.5784	12.575	12.579	12.579	12.5796	12.610	12.575	0.057	0.0471	0.052	0.003
b(2)	12.6652	12.663	12.665	12.665	12.6671	12.694	12.663	0.126	0.1186	0.124	0.006
b(3)	12.7532	12.750	12.754	12.754	12.7598	12.784	12.750	0.230	0.2194	0.217	0.007
G(0)	12.8097			12.814		12.842	12.810	0.500		0.603	0.151
b(4)	*12.8384*	*12.835*	*12.839*	*12.839*	*12.8559*	*12.861*	*12.835*	*0.359*	*0.2995*	*0.283*	*0.021*
D(0)	*12.8414*			*12.842*	*12.8412*	*12.868*	*12.841*	*0.9819*		*0.985*	
b'(0)	12.8535		12.854		12.8574	12.887	12.861	0.006	0.0000	0.005	0.001
c(0)	12.9115	12.910	12.912	12.914	12.920	12.938	12.910	0.630	0.5018	0.495	0.030
c'(0)	12.9344	12.935	12.935	12.936	12.9487	12.964	12.935	0.750	0.7651	0.786	0.028
b'(1)	12.9463		12.946		12.951	12.976	12.956	0.012	0.0025	0.049	0.006
b(5)	*12.9811*	*12.980*	*12.981*	*12.981*	*12.9538*	*13.021*	*12.950*	*0.018*	0.0123	*0.012*	*0.008*
F(0)	*12.9849*					*12.784*	*12.980*	*0.264*		*0.603*	
b'(2)	13.0371		13.037		13.0427	13.067	13.049	0.010	0.0003	0.001	0.000
b(6)	13.0612	13.062	13.061	13.061	13.0522	13.086	13.062	0.016	*0.0188*	0.032	0.011
o(0)	*13.103*	*13.100*	*13.103*	*13.103*	*13.103*	*13.131*	*13.100*	*0.007*	*0.0152*	*0.024*	*0.024*
D(1)	*13.1066*				*13.112*		*13.097*	*0.0176*		*0.015*	
b'(3)	13.1261		13.126		13.1339	13.156	13.142	0.007	0.0006	0.002	0.000
b(7)	13.1559	13.156	13.156	13.156	13.1504	13.180	13.156	0.089	0.1051	0.091	0.012
G(1)	13.1625					13.086	13.06	0.500		0.182	0.046
c'(1)	13.1881	13.185	13.188		13.216	13.208	13.185	0.007	0.0436	0.052	0.003
c(1)	*13.2078*	*13.210*	*13.208*	*13.215*	*13.211*	*13.227*	*13.210*	*0.088*	0.3975	*0.391*	*0.116*
F(1)	*13.212*					*13.021*	*13.210*	*0.373*		*0.182*	
b'(4)	13.2225		13.223		13.2242	13.240	13.232	0.036	0.0103	0.002	0.002
b(8)	13.258	13.260	13.258	13.258	13.2474	13.285	13.260	0.002	0.0074	0.005	0.001
b'(5)	13.3068	13.305	13.307		13.3136	13.330	13.322	0.005	*0.0047*	0.002	0.000
o(1)	*13.3445*	*13.345*	*13.345*	*13.346*	*13.346*	*13.367*	*13.345*	*0.178*	*0.3833*	*0.346*	*0.112*
b(9)	*13.3468*	*13.345*	*13.346*	*13.346*	*13.3429*	*13.364*	*13.345*	*0.017*	*0.0274*	*0.026*	*0.016*
D(2)	13.3679				13.3791	13.234		0.000		*0.000*	
b'(6)	*13.3902*	*13.390*	*13.390*	*13.396*	*13.4022*	*13.408*	*13.410*	*0.012*	0.0069	*0.003*	*0.001*
G(2)	*13.394*			*13.396*				*0.000*		*0.219*	*0.055*
b(10)	13.4364	13.435	13.437	13.437	13.4365	13.452	13.435	0.050	0.0444	0.054	0.007
c'(2)	13.4579		13.458		13.478	13.478	13.459	0.003	0.0059	0.003	0.005
F(2)	13.468						13.430	0.219		0.219	
c(2)	13.4764	13.475	13.476	13.477	13.476	13.491	13.475	0.104	0.0902	0.110	0.012
b'(7)	13.5082		13.508		13.4899	13.529	13.498	0.103	0.0009	0.001	0.000
b(11)	13.5291	13.529	13.529		13.5280	13.548	13.530	0.017	0.0243	0.020	0.001
b'(8)	*13.5817*		*13.582*	*13.582*	*13.577*	*13.600*	*13.583*	*0.014*	*0.0131*	*0.011*	*0.006*
o(2)	*13.5839*	*13.585*	*13.584*	*13.584*	*13.585*	*13.600*	*13.585*	*0.373*	*0.3472*	*0.225*	*0.169*
b(12)	13.6174	13.615	13.617		13.6172	13.632	13.615	0.003	0.0083	0.014	0.004
D(3)	13.6254				13.642			0.000		0.000	
G(3)	13.635							0.000		0.099	0.025
b'(9)	13.6627	13.660	13.663	13.663	13.6627	13.672	13.668	0.135	0.0316	0.008	0.001
b(13)	13.7041	13.700	13.704		13.7041	13.716	13.700	0.001	0.0120	0.033	0.009
c'(3)	13.7207	13.720	13.720	13.720	13.734	13.729	13.720	0.045	0.0328	0.007	0.004
F(3)	13.729					13.452		0.115		0.099	
c(3)	13.7368		13.737	13.737	13.737	13.729	13.722	0.006	*0.0106*	0.004	0.001
b'(10)	13.7554	13.760	13.755	13.755	13.7478	13.7220	13.751	0.160	*0.0166*	0.004	0.001
b(14)	13.7884	13.785	13.788		13.789	13.793	13.785	0.003	0.0216	0.004	0.004
o(3)	13.8194	13.830	13.818		13.820	13.831	13.820	0.328	0.1717	0.323	0.204

Table 1.

Angle (degrees)	17.5eV		20eV		30eV		50eV		100eV	
	R	Total DCS	R	Total DCS	R	Total DCS	R	Total DCS	R	Total DCS
2									0.749	1000
3							0.296	325	0.594	747
5			0.0298	20.1	7.79E-17	75.2	0.228	235	0.344	378
8							0.161	153	0.181	159
10	0.00709	3.83	0.0232	14.1	5.22E-17	49.9	0.133	114	0.111	82.2
12							0.106	80	0.068	42.3
15	0.00734	3.47	0.0199	10.7	3.39E-17	32.4	0.0738	44.8	0.0432	20.4
18									0.0328	11.4
20	0.00758	3.06	0.0192	8.72	2.05E-17	19.6	0.0477	19.7	0.0306	8.59
25	0.00734	2.44	0.0168	6.09	1.16E-17	11.1	0.0398	11.3	0.0355	5.52
30	0.00722	1.93	0.0152	4.21	7.51E-18	7.08	0.0402	6.76	0.0477	3.88
35	0.0073	1.56	0.0147	3.08	5.26E-18	4.88	0.0488	5.45	0.0571	2.52
40	0.00734	1.26	0.0156	2.5	4.01E-18	3.64	0.0575	3.87	0.0574	1.59
45	0.00839	1.15	0.0161	2	3.51E-18	3.18	0.0678	3.11	0.0546	1.05
50	0.00995	1.1	0.0182	1.77	3.14E-18	2.88	0.0769	2.5	0.0479	0.687
55					2.66E-18				0.0465	0.543
60	0.0141	1.01	0.0269	1.57	2.34E-18	2.17	0.0717	1.27	0.0429	0.433
65									0.039	0.346
70	0.0228	1.02	0.0384	1.47	2.06E-18	1.85	0.0907	1.01		
80	0.0351	1.04	0.0614	1.46	1.85E-18	1.69	0.0947	0.738		
90	0.0345	0.812	0.0649	1.32	1.59E-18	1.44	0.0981	0.598		
100	0.024	0.673	0.0493	1.31	1.62E-18	1.45	0.0756	0.559		
110	0.0174	0.666	0.0338	1.27	1.52E-18	1.34	0.0557	0.618		
120	0.0131	0.663	0.0261	1.3	1.71E-18	1.53	0.0448	0.865		
130	0.0115	0.736	0.022	1.33	1.79E-18	1.65	0.0379	1.18		
Error	0.087	0.165	0.080	0.161	0.085	0.164	0.085	0.164	0.089	0.166

Table 2.

Table 3a.

Angle (degrees)	Total		$a''\,^1\Sigma_g^+$		$b\,^1\Pi_u$		$c\,^1\Pi_u$		$o\,^1\Pi_u$		$b'\,^1\Sigma_u^+$		$c'\,^1\Sigma_u^+$		$G\,^3\Pi_u$		$F\,^3\Pi_u$	
	DCS	Error	DCS	Error	DCS	Error	DCS	Error	DCS	Error	DCS	Error	DCS	Error	DCS	Error	DCS	Error
3	3.95	0.653	0.128	0.0231	1.41	0.276	0.716	0.147	0.291	0.065	0.716	0.167	0.588	0.139	0.0588	0.0155	0.0454	0.0126
5	3.96	0.653	0.566	0.102	1.29	0.253	0.657	0.134	0.27	0.0603	0.51	0.119	0.505	0.12	0.0917	0.0241	0.065	0.0181
8	3.91	0.645	0.86	0.154	1.19	0.232	0.514	0.105	0.215	0.0482	0.368	0.0855	0.558	0.132	0.129	0.0341	0.077	0.0214
10	3.83	0.632	0.833	0.15	1.11	0.217	0.615	0.126	0.202	0.0453	0.416	0.0967	0.422	0.1	0.146	0.0384	0.0817	0.0227
12	3.7	0.611	0.719	0.129	1.16	0.228	0.551	0.113	0.2	0.0448	0.42	0.0977	0.396	0.0937	0.16	0.042	0.0911	0.0254
15	3.47	0.573	0.551	0.099	1.2	0.235	0.535	0.109	0.219	0.049	0.378	0.0879	0.321	0.076	0.175	0.0461	0.0911	0.0254
18	3.25	0.537	0.465	0.0835	1.14	0.223	0.504	0.103	0.212	0.0475	0.347	0.0807	0.335	0.0793	0.151	0.0396	0.101	0.0282
20	3.06	0.505	0.392	0.0704	1.12	0.218	0.524	0.107	0.188	0.0421	0.318	0.0739	0.255	0.0603	0.167	0.0439	0.1	0.0279
25	2.44	0.403	0.251	0.0452	0.835	0.163	0.396	0.081	0.199	0.0445	0.345	0.0802	0.169	0.0401	0.166	0.0437	0.0842	0.0234
27	2.24	0.37	0.217	0.039	0.902	0.177	0.365	0.0748	0.164	0.0368	0.254	0.059	0.0973	0.0231	0.158	0.0416	0.0846	0.0235
30	1.93	0.318	0.187	0.0337	0.651	0.127	0.253	0.0518	0.156	0.0349	0.287	0.0669	0.115	0.0273	0.191	0.0503	0.0918	0.0255
35	1.56	0.257	0.183	0.0328	0.482	0.0943	0.179	0.0366	0.137	0.0307	0.239	0.0557	0.075	0.0178	0.194	0.0511	0.0768	0.0214
37	1.37	0.226	0.162	0.0292	0.46	0.0901	0.172	0.0352	0.101	0.0227	0.216	0.0504	0.0476	0.0113	0.15	0.0395	0.0653	0.0182
40	1.26	0.207	0.187	0.0335	0.394	0.0771	0.134	0.0274	0.102	0.0227	0.201	0.0468	0.0388	0.00919	0.144	0.0378	0.0619	0.0172
45	1.15	0.19	0.171	0.0307	0.326	0.0639	0.128	0.0263	0.102	0.0227	0.178	0.0415	0.0505	0.012	0.137	0.0361	0.0623	0.0173
50	1.1	0.181	0.17	0.0305	0.262	0.0512	0.11	0.0225	0.0899	0.0201	0.183	0.0426	0.0431	0.0102	0.171	0.045	0.0774	0.0215
55	1.03	0.17	0.15	0.0269	0.251	0.0491	0.11	0.0225	0.0844	0.0189	0.168	0.039	0.0468	0.0111	0.166	0.0437	0.0661	0.0184
60	1.01	0.166	0.146	0.0263	0.268	0.0524	0.0994	0.0203	0.0721	0.0161	0.167	0.0389	0.0427	0.0101	0.147	0.0387	0.0727	0.0202
65	1.03	0.171	0.121	0.0218	0.301	0.0589	0.136	0.0279	0.0778	0.0174	0.146	0.0339	0.0405	0.0096	0.147	0.0388	0.0713	0.0198
70	1.02	0.169	0.113	0.0203	0.31	0.0607	0.138	0.0283	0.0796	0.0178	0.133	0.0309	0.0602	0.0143	0.135	0.0357	0.057	0.0159
75	1.06	0.175	0.109	0.0196	0.351	0.0687	0.137	0.028	0.0959	0.0214	0.135	0.0313	0.0512	0.0121	0.125	0.0328	0.0609	0.0169
80	1.04	0.172	0.11	0.0198	0.366	0.0717	0.122	0.025	0.0977	0.0219	0.15	0.0349	0.0519	0.0123	0.102	0.0269	0.0463	0.0129
85	0.901	0.149	0.103	0.0185	0.327	0.064	0.097	0.0199	0.094	0.021	0.117	0.0273	0.0509	0.0121	0.0807	0.0212	0.0325	0.00906
90	0.812	0.134	0.103	0.0185	0.296	0.0578	0.0852	0.0174	0.0718	0.0161	0.109	0.0255	0.0519	0.0123	0.0701	0.0184	0.0267	0.00742
95	0.724	0.119	0.0905	0.0163	0.263	0.0515	0.0759	0.0155	0.0701	0.0157	0.0959	0.0223	0.0392	0.00929	0.06	0.0158	0.0297	0.00826
100	0.673	0.111	0.0875	0.0157	0.245	0.048	0.0789	0.0162	0.058	0.013	0.0834	0.0194	0.0451	0.0107	0.048	0.0126	0.0276	0.00768
105	0.679	0.112	0.106	0.0191	0.237	0.0464	0.063	0.0129	0.0624	0.014	0.0867	0.0202	0.0423	0.01	0.0518	0.0136	0.0301	0.00837
110	0.666	0.11	0.113	0.0203	0.216	0.0423	0.0653	0.0134	0.0604	0.0135	0.0996	0.0232	0.0474	0.0112	0.0431	0.0113	0.0219	0.00608
115	0.664	0.11	0.114	0.0205	0.22	0.043	0.0603	0.0124	0.0613	0.0137	0.112	0.026	0.0298	0.00706	0.0397	0.0104	0.0284	0.00789
120	0.663	0.109	0.133	0.0239	0.206	0.0403	0.0538	0.011	0.073	0.0163	0.103	0.0239	0.0264	0.00625	0.0418	0.011	0.0272	0.00758
125	0.674	0.111	0.125	0.0225	0.217	0.0424	0.0578	0.0118	0.0641	0.0143	0.108	0.0252	0.032	0.00759	0.048	0.0126	0.0221	0.00616
130	0.736	0.121	0.147	0.0265	0.199	0.0389	0.07	0.0143	0.0757	0.0169	0.119	0.0277	0.0408	0.00966	0.0598	0.0157	0.0254	0.00706
Fractional Error		0.165		0.180		0.196		0.205		0.224		0.233		0.237		0.263		0.278

Table 3b.

Angle (degrees)	Total		$a''\,^1\Sigma_g^+$		$b\,^1\Pi_u$		$c\,^1\Pi_u$		$o\,^1\Pi_u$		$b'\,^1\Sigma_u^+$		$c'\,^1\Sigma_u^+$		$G\,^3\Pi_u$		$F\,^3\Pi_u$	
	DCS	Error	DCS	Error	DCS	Error	DCS	Error	DCS	Error	DCS	Error	DCS	Error	DCS	Error	DCS	Error
3	23	3.71	0.922	0.162	6.23	1.18	4.39	0.855	2.37	0.493	4.53	0.979	3.85	0.875	0.534	0.144	0.2	0.0546
5	20.1	3.24	1.75	0.308	5.35	1.01	3.64	0.71	1.99	0.412	3.59	0.777	2.92	0.664	0.597	0.16	0.266	0.0726
8	16.6	2.68	2.08	0.366	4.8	0.907	2.71	0.527	1.41	0.294	2.71	0.585	2.09	0.474	0.551	0.148	0.295	0.0806
10	14.1	2.28	1.65	0.291	4.56	0.861	2.32	0.451	1.04	0.216	2.15	0.464	1.8	0.408	0.398	0.107	0.224	0.061
12	13.8	2.22	1.36	0.239	4.52	0.854	2.41	0.469	0.984	0.205	1.9	0.411	1.92	0.437	0.525	0.141	0.18	0.049
15	10.7	1.72	0.854	0.151	3.94	0.742	2.06	0.401	0.744	0.155	1.28	0.278	1.26	0.287	0.382	0.103	0.178	0.0485
18	9.51	1.53	0.614	0.108	3.57	0.673	1.56	0.304	0.69	0.143	1.6	0.346	0.967	0.22	0.363	0.0974	0.171	0.0466
20	8.72	1.41	0.454	0.0799	3.66	0.691	1.52	0.297	0.557	0.116	1.28	0.278	0.741	0.168	0.361	0.0971	0.165	0.0451
25	6.09	0.982	0.211	0.0372	2.61	0.493	1.05	0.205	0.464	0.0964	0.957	0.207	0.403	0.0916	0.303	0.0814	0.117	0.032
27	5.04	0.812	0.284	0.0501	1.93	0.364	0.919	0.179	0.416	0.0865	0.831	0.18	0.32	0.0728	0.242	0.0651	0.119	0.0324
30	4.21	0.678	0.247	0.0435	1.74	0.329	0.564	0.11	0.318	0.0661	0.715	0.155	0.256	0.0582	0.272	0.0731	0.125	0.0341
35	3.08	0.497	0.272	0.0479	1.19	0.225	0.346	0.0674	0.245	0.051	0.576	0.125	0.121	0.0275	0.256	0.0687	0.117	0.0319
37	2.78	0.449	0.301	0.053	1.13	0.213	0.263	0.0512	0.188	0.039	0.421	0.091	0.0996	0.0226	0.3	0.0806	0.145	0.0394
40	2.5	0.404	0.311	0.0549	0.994	0.188	0.26	0.0507	0.152	0.0317	0.314	0.0678	0.0938	0.0213	0.299	0.0804	0.146	0.0399
45	2	0.322	0.283	0.0499	0.756	0.143	0.238	0.0463	0.128	0.0267	0.245	0.0529	0.0756	0.0172	0.212	0.057	0.102	0.0278
50	1.77	0.285	0.229	0.0403	0.684	0.129	0.233	0.0454	0.142	0.0295	0.194	0.0419	0.0776	0.0176	0.147	0.0394	0.0918	0.025
55	1.65	0.265	0.219	0.0386	0.599	0.113	0.209	0.0408	0.127	0.0263	0.196	0.0423	0.0901	0.0205	0.142	0.0382	0.0942	0.0257
60	1.57	0.253	0.188	0.0332	0.591	0.112	0.241	0.0469	0.124	0.0258	0.156	0.0338	0.0934	0.0212	0.117	0.0315	0.0795	0.0217
65	1.52	0.245	0.182	0.0321	0.561	0.106	0.245	0.0476	0.114	0.0236	0.139	0.03	0.109	0.0248	0.118	0.0318	0.0733	0.02
70	1.47	0.237	0.156	0.0274	0.571	0.108	0.216	0.042	0.107	0.0223	0.172	0.0371	0.0988	0.0224	0.1	0.0269	0.0691	0.0189
75	1.46	0.236	0.139	0.0245	0.622	0.117	0.213	0.0414	0.122	0.0252	0.148	0.0319	0.0817	0.0186	0.097	0.0261	0.0546	0.0149
80	1.46	0.235	0.147	0.0258	0.588	0.111	0.189	0.0368	0.129	0.0269	0.188	0.0406	0.0949	0.0216	0.092	0.0247	0.0432	0.0118
85	1.39	0.224	0.137	0.0242	0.594	0.112	0.192	0.0373	0.135	0.0281	0.161	0.0347	0.0613	0.0139	0.0806	0.0217	0.0369	0.0101
90	1.32	0.214	0.159	0.028	0.485	0.0916	0.16	0.0312	0.143	0.0297	0.191	0.0412	0.069	0.0157	0.0901	0.0242	0.0391	0.0107
95	1.3	0.21	0.143	0.0252	0.482	0.0909	0.163	0.0318	0.162	0.0337	0.176	0.0379	0.0588	0.0134	0.0908	0.0244	0.0397	0.0108
100	1.31	0.211	0.145	0.0255	0.516	0.0974	0.132	0.0257	0.153	0.0319	0.18	0.0389	0.0719	0.0163	0.0802	0.0215	0.0375	0.0102
105	1.27	0.204	0.175	0.0308	0.447	0.0843	0.119	0.0232	0.165	0.0343	0.199	0.043	0.0554	0.0126	0.0839	0.0226	0.0307	0.00837
110	1.27	0.204	0.16	0.0281	0.426	0.0804	0.119	0.0232	0.139	0.0289	0.246	0.0533	0.0636	0.0144	0.0925	0.0249	0.0328	0.00894
115	1.29	0.208	0.18	0.0317	0.421	0.0795	0.114	0.0222	0.145	0.03	0.248	0.0536	0.0524	0.0119	0.107	0.0287	0.0377	0.0103
120	1.3	0.209	0.237	0.0418	0.413	0.0779	0.115	0.0225	0.134	0.0279	0.237	0.0512	0.0418	0.00949	0.0927	0.0249	0.0408	0.0111
125	1.31	0.212	0.256	0.0451	0.424	0.0801	0.112	0.0218	0.128	0.0266	0.224	0.0484	0.0459	0.0104	0.0893	0.024	0.0468	0.0128
130	1.33	0.215	0.283	0.0498	0.454	0.0857	0.114	0.0223	0.118	0.0245	0.201	0.0434	0.0426	0.00969	0.0795	0.0214	0.0517	0.0141
Fractional Error		0.161		0.196		0.205		0.224		0.233		0.237		0.263		0.278		0.273

Table 3c.

Angle (degrees)	Total		$a''\,^1\Sigma_g^+$		$b\,^1\Pi_u$		$c\,^1\Pi_u$		$o\,^1\Pi_u$		$b'\,^1\Sigma_u^+$		$c'\,^1\Sigma_u^+$		$G\,^3\Pi_u$		$F\,^3\Pi_u$	
	DCS	Error	DCS	Error	DCS	Error	DCS	Error	DCS	Error	DCS	Error	DCS	Error	DCS	Error	DCS	Error
2	96.2	15.8	4.77	0.912	34.3	6.92	17.5	3.61	5.53	1.16	16.3	3.56	14.6	3.33	1.76	0.447	1.58	0.431
3	89.9	14.7	4.65	0.89	31.9	6.44	16.4	3.39	4.81	1.01	15.3	3.34	13.9	3.17	1.71	0.436	1.23	0.336
4	86	14.1	4.13	0.791	32.3	6.53	14.1	2.9	4.03	0.846	12.9	2.82	15.5	3.55	1.68	0.429	1.41	0.384
5	77.8	12.7	3.74	0.717	26.3	5.31	14.6	3.01	3.53	0.74	13.7	2.99	13.3	3.04	1.55	0.394	1.17	0.319
6	72.7	11.9	3.06	0.587	27.7	5.59	11.8	2.42	3.34	0.699	10.7	2.33	13.5	3.09	1.48	0.378	1.36	0.37
8	60.2	9.87	2.27	0.435	24.7	4.99	9.97	2.05	2.95	0.618	7.77	1.69	10.3	2.36	1.3	0.331	1.03	0.279
10	52.1	8.53	1.57	0.301	21	4.23	9.27	1.91	2.48	0.52	7.08	1.54	8.55	1.96	1.21	0.308	1.08	0.293
12	42.7	7	0.986	0.189	18.4	3.72	7.04	1.45	1.98	0.415	5.53	1.21	7.03	1.61	1.01	0.256	0.798	0.217
15	33.8	5.54	0.473	0.0906	14	2.83	7.09	1.46	2.27	0.477	5.04	1.1	3.51	0.803	0.813	0.207	0.661	0.18
18	24.5	4.02	0.241	0.0461	11.1	2.24	4.63	0.955	1.55	0.324	3.82	0.834	2.17	0.496	0.61	0.155	0.473	0.128
20	20.5	3.36	0.169	0.0323	10	2.02	3.62	0.747	1.42	0.298	2.71	0.592	1.68	0.384	0.544	0.139	0.394	0.107
25	11.6	1.9	0.224	0.043	5.5	1.11	1.98	0.408	1.07	0.224	1.64	0.357	0.652	0.149	0.318	0.0809	0.254	0.069
27	9.99	1.64	0.277	0.053	4.96	1	1.78	0.366	0.976	0.205	0.955	0.208	0.556	0.127	0.298	0.076	0.219	0.0595
30	7.48	1.23	0.249	0.0476	3.7	0.748	1.27	0.262	0.704	0.148	0.767	0.167	0.387	0.0885	0.24	0.061	0.184	0.05
35	5.23	0.857	0.294	0.0563	2.34	0.472	0.904	0.186	0.466	0.0977	0.519	0.113	0.353	0.0808	0.214	0.0546	0.168	0.0458
36	4.86	0.795	0.266	0.0509	2.26	0.456	0.841	0.173	0.367	0.077	0.41	0.0894	0.356	0.0816	0.217	0.0554	0.168	0.0456
40	3.98	0.652	0.285	0.0545	1.57	0.316	0.683	0.141	0.334	0.0701	0.401	0.0874	0.373	0.0855	0.211	0.0538	0.158	0.0429
45	3.48	0.57	0.248	0.0475	1.41	0.285	0.537	0.111	0.21	0.0441	0.418	0.0912	0.355	0.0813	0.19	0.0485	0.136	0.0369
50	3.12	0.511	0.23	0.044	1.17	0.236	0.576	0.119	0.205	0.043	0.395	0.0861	0.301	0.069	0.185	0.0471	0.0809	0.022
55	2.64	0.433	0.195	0.0372	1.08	0.218	0.445	0.0918	0.154	0.0322	0.34	0.0742	0.236	0.054	0.118	0.0301	0.0921	0.025
60	2.33	0.382	0.17	0.0325	0.943	0.19	0.395	0.0814	0.138	0.029	0.296	0.0646	0.228	0.0521	0.101	0.0256	0.074	0.0201
65	2.11	0.345	0.168	0.0321	0.849	0.171	0.314	0.0647	0.15	0.0314	0.247	0.0538	0.245	0.0561	0.0803	0.0205	0.0632	0.0172
70	2.04	0.334	0.136	0.0261	0.91	0.184	0.299	0.0616	0.124	0.0261	0.244	0.0532	0.187	0.0429	0.0873	0.0222	0.0675	0.0183
75	1.88	0.308	0.125	0.024	0.851	0.172	0.258	0.0532	0.129	0.027	0.22	0.048	0.16	0.0367	0.0861	0.0219	0.062	0.0169
80	1.84	0.301	0.13	0.0249	0.925	0.187	0.222	0.0458	0.126	0.0264	0.161	0.0351	0.125	0.0287	0.0945	0.0241	0.0661	0.018
85	1.77	0.29	0.116	0.0221	0.89	0.18	0.202	0.0416	0.113	0.0236	0.183	0.0399	0.114	0.0262	0.0968	0.0246	0.0718	0.0195
90	1.58	0.259	0.123	0.0235	0.743	0.15	0.166	0.0342	0.129	0.027	0.154	0.0336	0.127	0.0291	0.0864	0.022	0.0647	0.0176
95	1.61	0.263	0.139	0.0267	0.728	0.147	0.174	0.0359	0.132	0.0276	0.149	0.0326	0.12	0.0276	0.109	0.0278	0.0798	0.0217
100	1.61	0.263	0.169	0.0323	0.73	0.147	0.195	0.0402	0.145	0.0304	0.0977	0.0213	0.109	0.0249	0.112	0.0285	0.068	0.0185
105	1.57	0.257	0.187	0.0358	0.611	0.123	0.192	0.0396	0.173	0.0362	0.101	0.022	0.15	0.0345	0.0962	0.0245	0.0738	0.0201
110	1.5	0.246	0.201	0.0386	0.535	0.108	0.178	0.0366	0.153	0.0322	0.122	0.0266	0.15	0.0344	0.105	0.0266	0.0756	0.0206
115	1.54	0.252	0.239	0.0458	0.574	0.116	0.172	0.0354	0.167	0.0351	0.118	0.0257	0.114	0.0261	0.0943	0.024	0.0753	0.0205
120	1.69	0.277	0.29	0.0555	0.568	0.115	0.2	0.0413	0.13	0.0273	0.184	0.0401	0.157	0.036	0.109	0.0278	0.0691	0.0188
125	1.7	0.279	0.337	0.0646	0.523	0.105	0.188	0.0387	0.15	0.0315	0.202	0.044	0.171	0.0391	0.0904	0.023	0.0543	0.0148
130	1.78	0.291	0.35	0.0669	0.538	0.109	0.197	0.0406	0.171	0.0316	0.256	0.0558	0.138	0.0316	0.0913	0.0233	0.0458	0.0124
Fractional Error		0.164		0.191		0.202		0.206		0.185		0.218		0.229		0.255		0.272

Table 3d.

Angle (degrees)	Total		$a''\,^1\Sigma_g^+$		$b\,^1\Pi_u$		$c\,^1\Pi_u$		$o\,^1\Pi_u$		$b'\,^1\Sigma_u^+$		$c'\,^1\Sigma_u^+$		$G\,^3\Pi_u$		$F\,^3\Pi_u$	
	DCS	Error	DCS	Error	DCS	Error	DCS	Error	DCS	Error	DCS	Error	DCS	Error	DCS	Error	DCS	Error
2	387	63.4	9.5	1.82	135	28.1	74.6	15.8	23.5	5.04	81.8	18.7	57.3	13.8	3.21	0.873	2.23	0.655
3	325	53.3	8.58	1.64	119	24.7	64.7	13.7	21.2	4.54	56.2	12.8	49.4	11.9	3.78	1.03	2.61	0.77
4	275	45.1	5.81	1.11	97.4	20.2	54.3	11.5	17.8	3.81	52.3	11.9	43.3	10.4	2.74	0.745	1.9	0.558
5	235	38.5	4.68	0.896	82.1	17.1	47.4	10.1	18.5	3.96	40.1	9.16	36.9	8.89	3.12	0.848	2.37	0.696
6	209	34.2	3.81	0.729	76.5	15.9	39.4	8.36	16.5	3.53	40.7	9.3	27.7	6.69	2.43	0.66	2.32	0.682
8	153	25	2.45	0.469	56.8	11.8	30.2	6.41	11.9	2.54	26.8	6.11	21.9	5.28	1.52	0.413	1.35	0.397
10	114	18.7	1.38	0.264	42.8	8.89	22.3	4.72	10.1	2.17	20.2	4.61	14.7	3.54	1.51	0.411	1.17	0.344
12	80	13.1	0.814	0.156	30.9	6.43	15.8	3.36	7.27	1.56	13.6	3.11	9.46	2.28	1.33	0.361	0.766	0.226
15	44.8	7.33	0.256	0.049	19.2	3.98	8.37	1.78	3.92	0.84	6.97	1.59	4.66	1.12	0.965	0.262	0.491	0.145
18	27.3	4.47	0.129	0.0246	11.7	2.44	4.91	1.04	2.78	0.596	4.79	1.09	2.04	0.492	0.634	0.172	0.284	0.0837
20	19.7	3.23	0.0698	0.0134	8.89	1.85	3.57	0.758	1.7	0.363	3.57	0.816	1.23	0.297	0.491	0.134	0.227	0.0669
25	11.3	1.86	0.11	0.0211	5.48	1.14	1.85	0.392	0.884	0.189	1.46	0.332	1.09	0.263	0.32	0.0869	0.171	0.0502
27	9.22	1.51	0.135	0.0258	4.24	0.881	1.52	0.323	0.817	0.175	1.28	0.291	0.816	0.197	0.275	0.0748	0.152	0.0448
30	6.76	1.11	0.209	0.04	2.95	0.612	1.19	0.253	0.549	0.118	0.914	0.209	0.624	0.151	0.213	0.0579	0.128	0.0378
35	5.45	0.892	0.248	0.0475	1.99	0.414	0.94	0.2	0.495	0.106	0.918	0.21	0.576	0.139	0.181	0.0491	0.108	0.0317
36	5.04	0.826	0.253	0.0484	1.91	0.396	0.95	0.202	0.348	0.0745	0.716	0.163	0.598	0.144	0.184	0.05	0.0934	0.0275
37	4.56	0.747	0.278	0.0532	1.59	0.331	0.86	0.183	0.41	0.0878	0.745	0.17	0.428	0.103	0.151	0.0411	0.0857	0.0252
40	3.87	0.634	0.238	0.0455	1.29	0.269	0.674	0.143	0.365	0.0782	0.597	0.136	0.479	0.115	0.161	0.0436	0.0743	0.0219
45	3.11	0.509	0.2	0.0383	1.03	0.215	0.498	0.106	0.315	0.0674	0.475	0.108	0.396	0.0956	0.124	0.0336	0.0746	0.022
50	2.5	0.41	0.221	0.0423	0.821	0.171	0.359	0.0761	0.253	0.0542	0.346	0.0791	0.348	0.0838	0.104	0.0282	0.0578	0.017
55	1.96	0.321	0.148	0.0282	0.743	0.155	0.302	0.064	0.177	0.0378	0.243	0.0555	0.215	0.0519	0.0878	0.0239	0.0426	0.0126
60	1.27	0.208	0.126	0.0241	0.45	0.0935	0.176	0.0373	0.122	0.0262	0.175	0.04	0.126	0.0305	0.0547	0.0149	0.0253	0.00745
65	1.25	0.205	0.094	0.018	0.466	0.0969	0.176	0.0373	0.122	0.0262	0.175	0.04	0.126	0.0305	0.058	0.0158	0.0308	0.00908
70	1.01	0.165	0.0974	0.0186	0.389	0.0809	0.131	0.0278	0.102	0.0219	0.147	0.0335	0.0654	0.0158	0.0501	0.0136	0.0283	0.00835
75	0.855	0.14	0.0737	0.0141	0.36	0.0748	0.12	0.0255	0.0667	0.0143	0.12	0.0275	0.0523	0.0126	0.0425	0.0116	0.0202	0.00594
80	0.738	0.121	0.0701	0.0134	0.293	0.0608	0.0944	0.02	0.0741	0.0159	0.101	0.023	0.0583	0.0141	0.0343	0.00932	0.0153	0.00452
85	0.638	0.105	0.0653	0.0125	0.242	0.0503	0.0789	0.0167	0.0556	0.0119	0.116	0.0265	0.0426	0.0103	0.0286	0.00777	0.0119	0.00351
90	0.598	0.098	0.063	0.0121	0.245	0.0509	0.0575	0.0122	0.0525	0.0112	0.085	0.0194	0.0557	0.0134	0.0298	0.00809	0.0126	0.00372
95	0.59	0.0967	0.0543	0.0104	0.253	0.0526	0.065	0.0138	0.0505	0.0108	0.0737	0.0168	0.0458	0.011	0.0313	0.00852	0.0188	0.00555
100	0.559	0.0916	0.0516	0.00988	0.217	0.0451	0.0614	0.013	0.055	0.0118	0.0686	0.0156	0.0629	0.0152	0.0278	0.00757	0.0146	0.00429
105	0.576	0.0944	0.0569	0.0109	0.202	0.042	0.0481	0.0102	0.0549	0.0118	0.0838	0.0191	0.0884	0.0213	0.0268	0.00727	0.0161	0.00475
110	0.618	0.101	0.0705	0.0135	0.221	0.0459	0.0617	0.0131	0.0624	0.0134	0.0846	0.0193	0.0722	0.0174	0.0308	0.00836	0.0174	0.00511
115	0.725	0.119	0.122	0.0233	0.228	0.0474	0.0554	0.0118	0.0754	0.0161	0.081	0.0185	0.104	0.025	0.0421	0.0114	0.0203	0.00598
120	0.865	0.142	0.149	0.0285	0.263	0.0546	0.078	0.0166	0.0815	0.0175	0.0958	0.0219	0.119	0.0286	0.0545	0.0148	0.0276	0.00812
125	1.05	0.172	0.189	0.0362	0.268	0.0558	0.0741	0.0157	0.138	0.0296	0.0983	0.0224	0.2	0.0481	0.061	0.0166	0.0269	0.00791
130	1.18	0.194	0.273	0.0522	0.326	0.0677	0.101	0.0214	0.129	0.0277	0.134	0.0306	0.115	0.0279	0.0765	0.0208	0.0282	0.00829
Fractional Error		0.164		0.191		0.208		0.212		0.214		0.228		0.241		0.272		0.294

Angle (degrees)	Total		$a''\ ^1\Sigma_g^+$		$b\ ^1\Pi_u$		$c\ ^1\Pi_u$		$o\ ^1\Pi_u$		$b'\ ^1\Sigma_u^+$		$c'\ ^1\Sigma_u^+$		$G\ ^3\Pi_u$		$F\ ^3\Pi_u$	
	DCS	Error	DCS	Error	DCS	Error	DCS	Error	DCS	Error	DCS	Error	DCS	Error	DCS	Error	DCS	Error
2	1000	166	12	2.43	340	70.3	202	42.7	93.6	19.5	178	41.5	171	41.9	3.62	1.1	1.5	0.498
3	747	124	8.79	1.79	257	53.1	147	31	76.1	15.9	120	28	132	32.4	3.77	1.15	2.23	0.743
4	557	92.5	7.33	1.49	201	41.6	106	22.3	56.9	11.9	91.9	21.5	89.2	21.9	3.22	0.978	2.08	0.693
5	378	62.8	4.5	0.914	135	27.9	70.1	14.8	36.1	7.51	56.3	13.1	71.4	17.5	3.17	0.963	1.98	0.658
6	284	47.1	3.34	0.678	101	20.9	53	11.2	29.3	6.11	39.8	9.29	52.7	12.9	2.72	0.826	2.11	0.702
8	159	26.4	2.09	0.425	60.2	12.4	30	6.32	15.3	3.2	21.9	5.11	26.5	6.5	1.62	0.491	1.38	0.459
10	82.2	13.7	0.998	0.203	31.5	6.51	15.2	3.2	9.04	1.88	10	2.34	14	3.43	0.788	0.239	0.816	0.271
12	42.3	7.02	0.515	0.105	18.5	3.82	7.73	1.63	3.95	0.824	5.66	1.32	5.31	1.3	0.354	0.108	0.262	0.0872
15	20.4	3.38	0.222	0.0451	9.17	1.9	3.41	0.72	1.99	0.414	2.81	0.656	2.38	0.585	0.219	0.0667	0.152	0.0504
18	11.4	1.9	0.136	0.0276	5.6	1.16	1.77	0.373	1.1	0.229	1.48	0.344	1.13	0.276	0.137	0.0416	0.085	0.0283
20	8.59	1.43	0.168	0.0341	3.95	0.816	1.2	0.252	0.849	0.177	1.2	0.281	1.03	0.253	0.123	0.0375	0.0746	0.0248
25	5.52	0.917	0.306	0.0621	2.09	0.432	0.696	0.147	0.598	0.125	0.797	0.186	0.911	0.223	0.0827	0.0251	0.0421	0.014
27	4.82	0.8	0.344	0.0699	1.51	0.313	0.761	0.16	0.58	0.121	0.751	0.175	0.761	0.187	0.075	0.0228	0.0342	0.0114
30	3.88	0.645	0.333	0.0677	1.25	0.258	0.619	0.131	0.447	0.0931	0.628	0.147	0.516	0.127	0.0605	0.0184	0.032	0.0106
35	2.52	0.418	0.3	0.061	0.716	0.148	0.4	0.0844	0.317	0.0661	0.421	0.0982	0.287	0.0705	0.0422	0.0128	0.0343	0.0114
37	2.03	0.338	0.24	0.0488	0.648	0.134	0.281	0.0592	0.252	0.0526	0.258	0.0601	0.297	0.0729	0.0367	0.0112	0.0227	0.00755
40	1.59	0.264	0.183	0.0372	0.481	0.0993	0.222	0.0468	0.184	0.0383	0.29	0.0677	0.185	0.0453	0.0305	0.00927	0.0217	0.00722
45	1.05	0.174	0.13	0.0264	0.305	0.0631	0.16	0.0337	0.116	0.0241	0.207	0.0483	0.098	0.024	0.0188	0.00572	0.0156	0.00519
50	0.687	0.114	0.102	0.0207	0.217	0.0449	0.0625	0.0132	0.0886	0.0185	0.103	0.024	0.0855	0.021	0.0188	0.00573	0.00937	0.00312
55	0.543	0.0902	0.0822	0.0167	0.19	0.0392	0.0757	0.016	0.0553	0.0115	0.0521	0.0121	0.0584	0.0143	0.0216	0.00655	0.00943	0.00313
Fractional Error		0.166		0.203		0.207		0.211		0.208		0.233		0.245		0.304		0.333

Figure 3e.

Table 4.

State	Centroid Diabatic (eV)	OOS [7] Diabatic	Centroid Adiabatic (eV)	OOS [7] Adiabatic	Centroid (P) eV	AOOS (P)	Error	AOOS (P) Corrected	Error	Correction Factor	AOOS [10,19]	Error	OOS [45]	AOOS (L) [18]	Error	OOS [46]	Error	OOS [47]	Error
b $^1\Pi_u$	12.955	0.279	13.201	0.124	12.636	0.115	0.026	0.117	0.026	0.98			0.160						
c $^1\Pi_u$	13.091	0.033	12.950	0.141	13.093	0.086	0.020	0.086	0.020	1.00	0.080	0.040							
o $^1\Pi_u$	13.584	0.009	13.680	0.061	12.533	0.043	0.011	0.047	0.013	0.92	0.026	0.013							
b′ $^1\Sigma_u^+$	13.316	0.221	14.197	0.209	13.166	0.079	0.021	0.927	0.252	0.085	0.120	0.060							
c′ $^1\Sigma_u^+$	13.001	0.113	13.000	0.139	12.958	0.069	0.020	0.081	0.023	0.85						0.136	0.020	0.156	0.030
Summed		0.655		0.674		0.392	0.099	1.259	0.335					0.6	0.1				

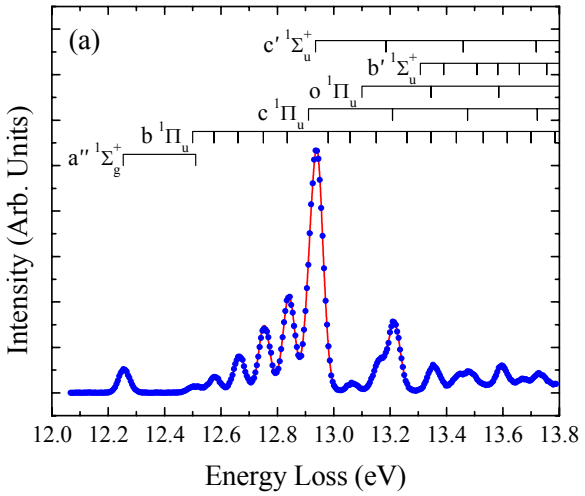

Figure 1 a.

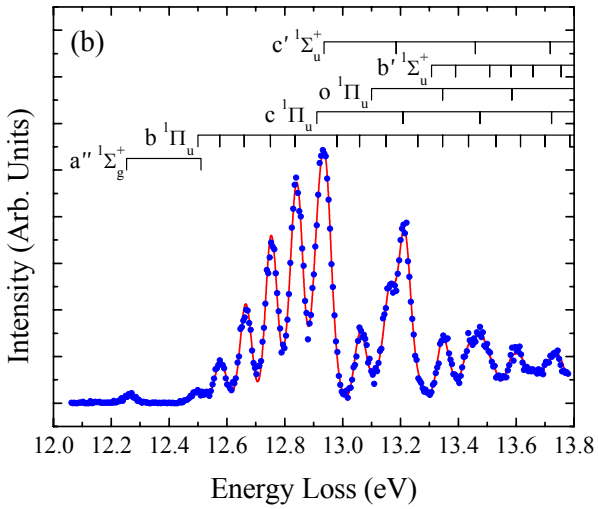

Figure 1b.

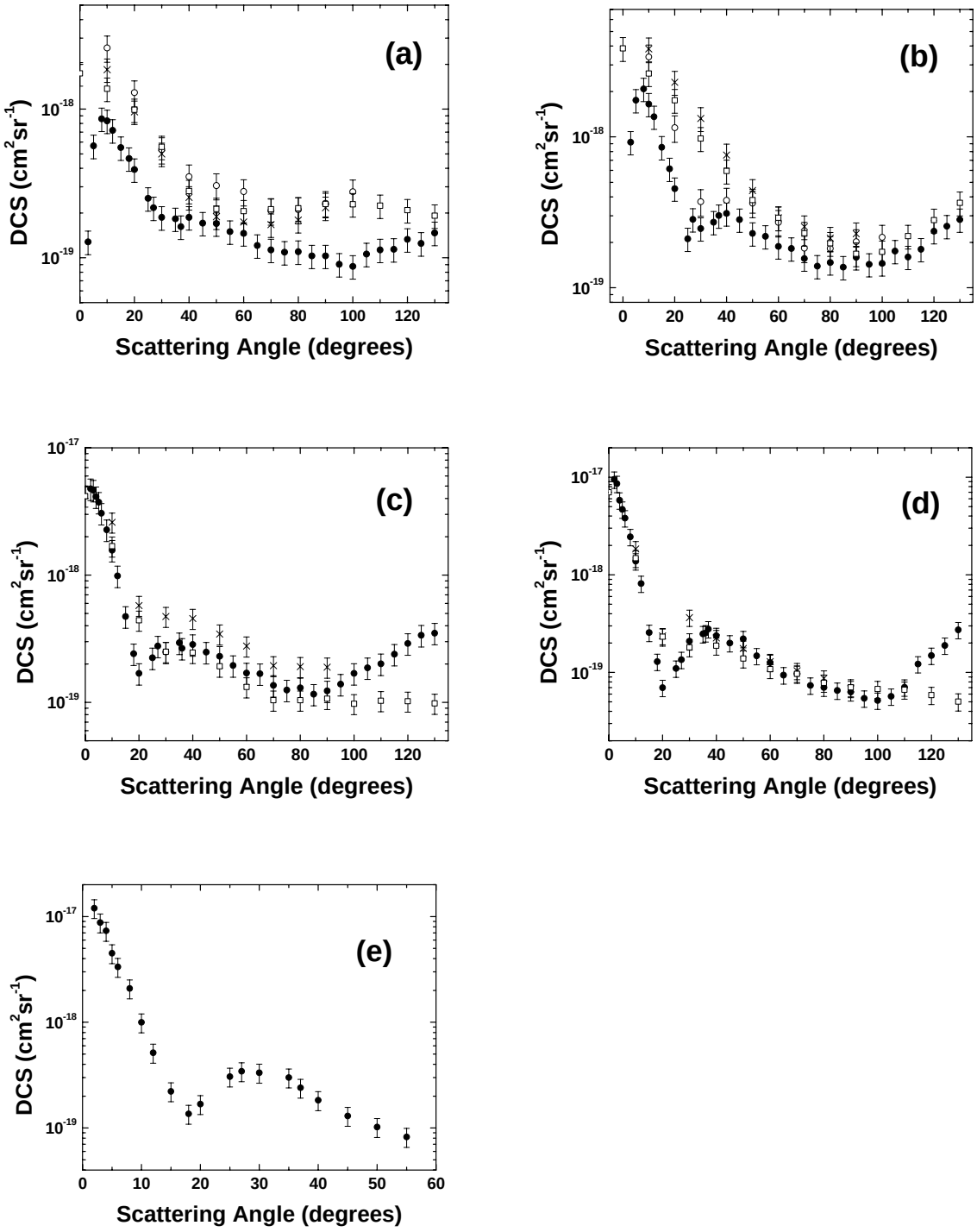

Figures 2a to 2e.

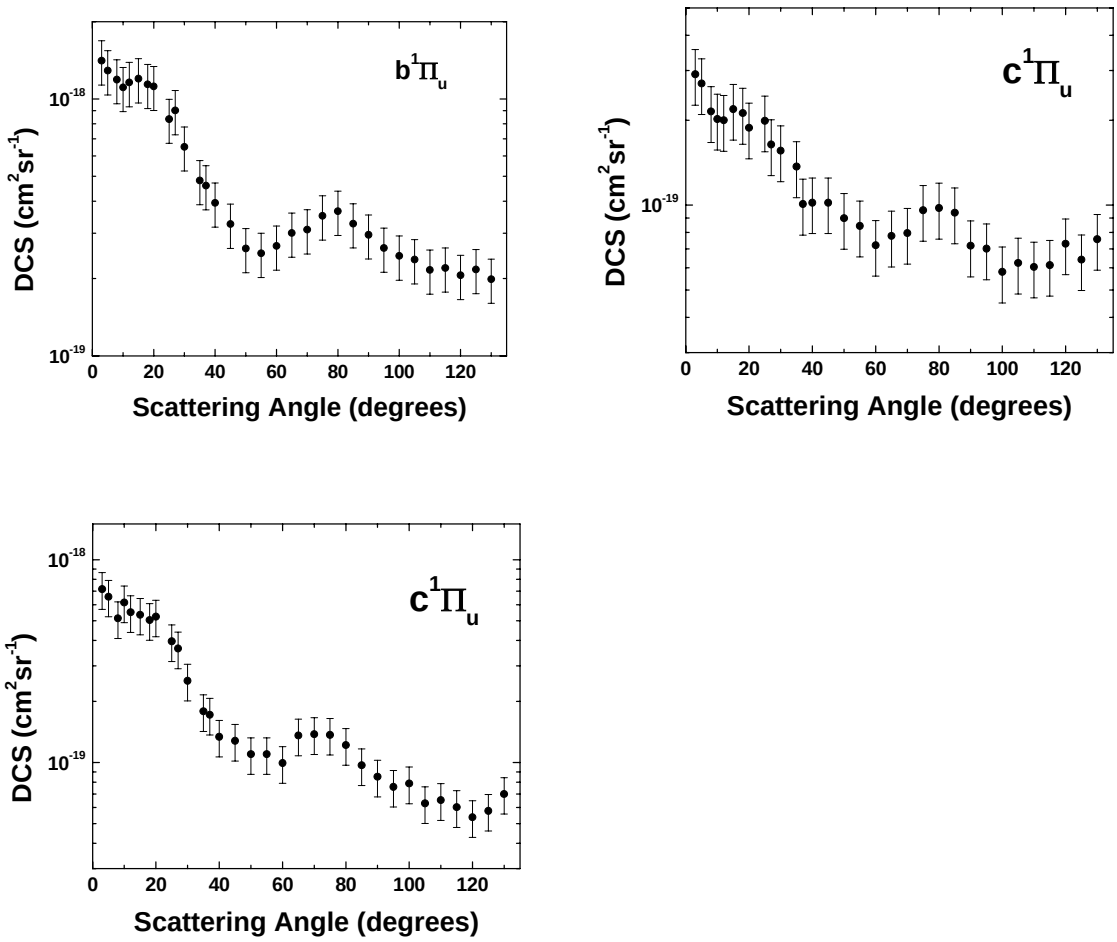
b¹Π_u
c¹Π_u
c¹Π_u
DCS (cm²sr⁻¹)
10⁻¹⁸
10⁻¹⁹
0
20
40
60
80
100
120
Scattering Angle (degrees)

Figures 3.

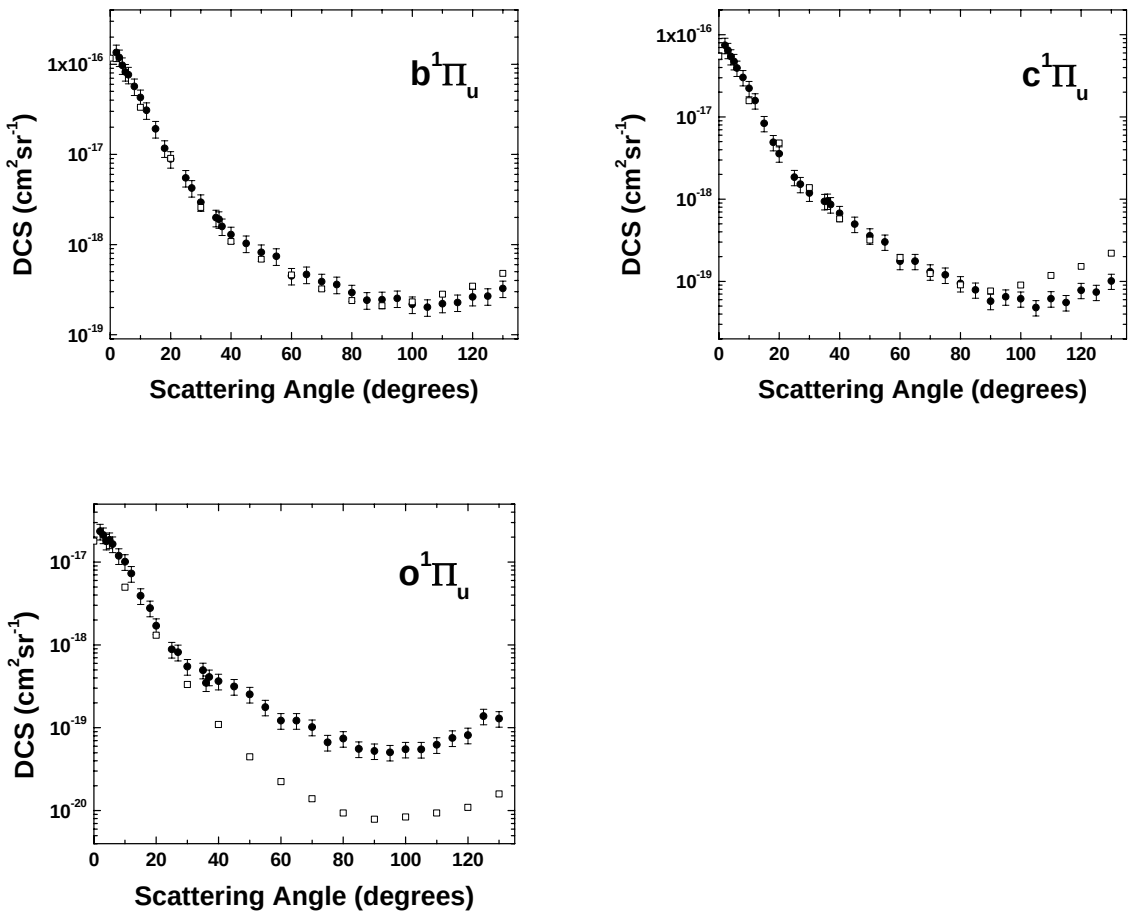

Figure 4.

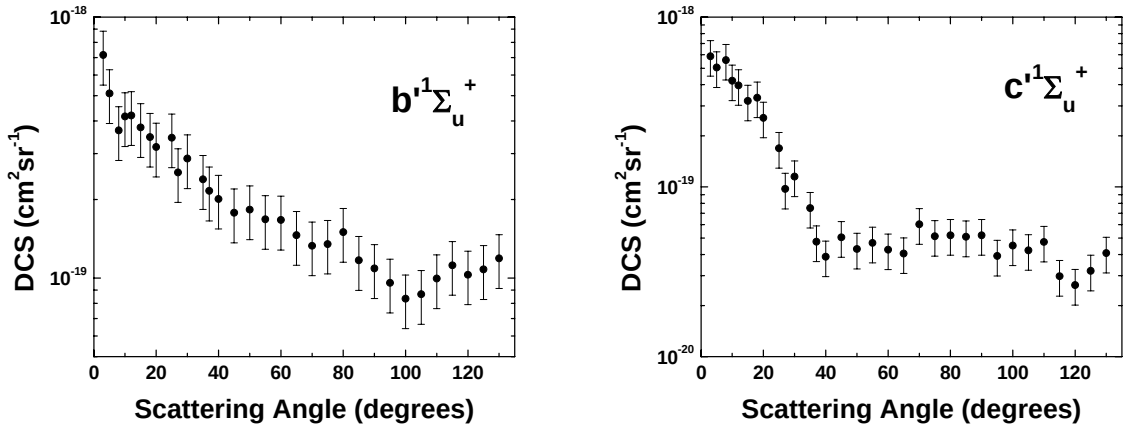

Figure 5.

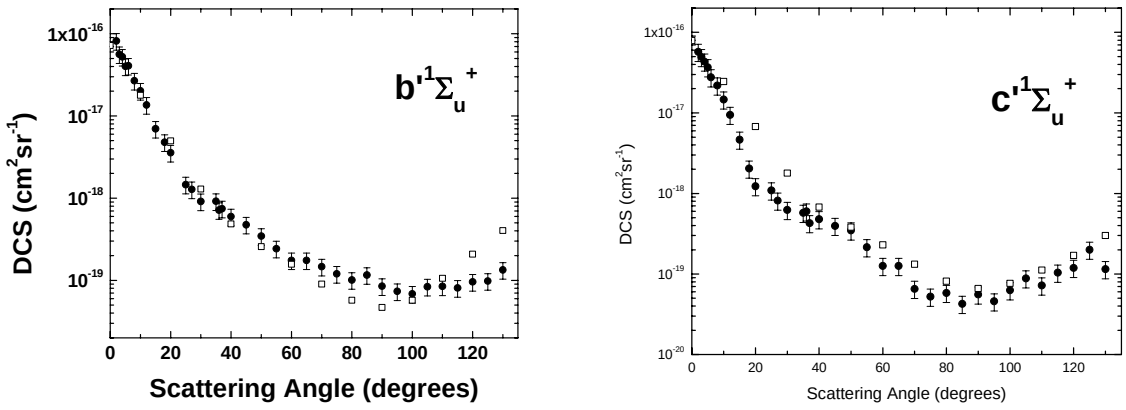

Figure 6.

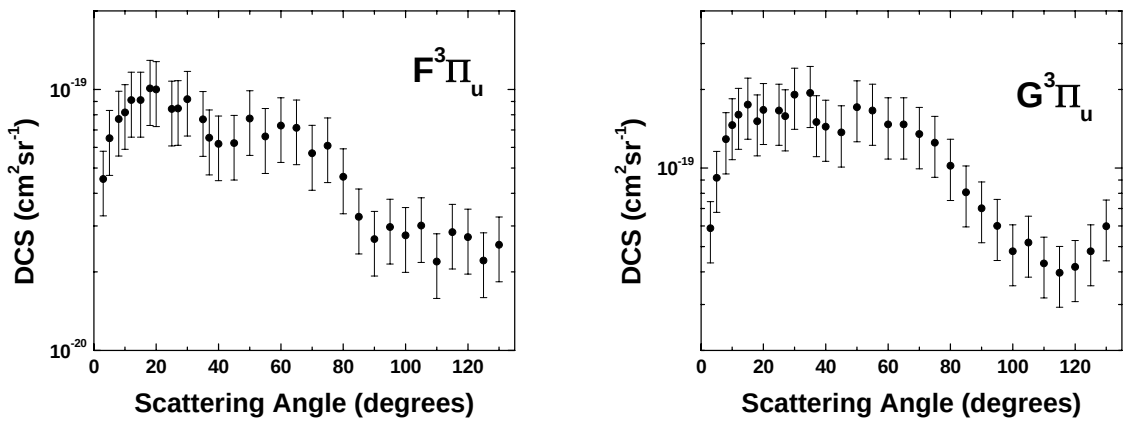

Figure 7.

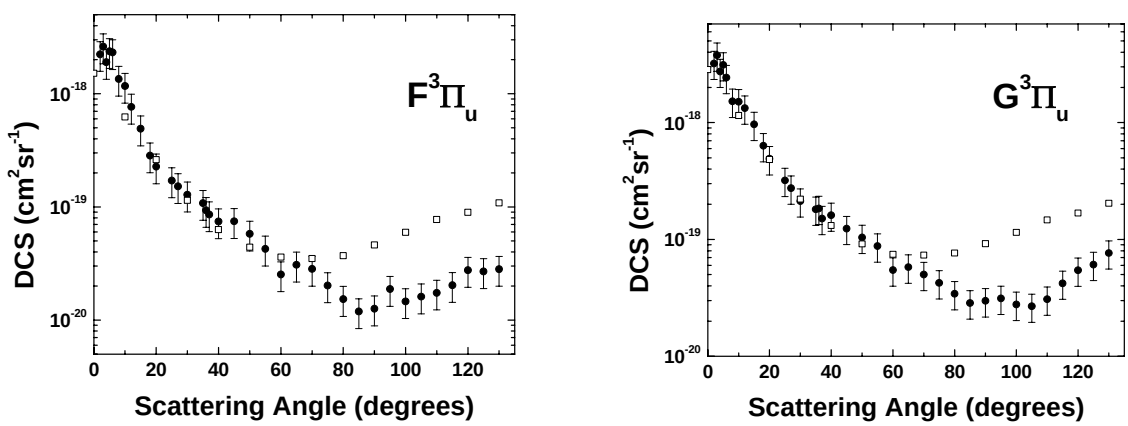

Figure 8.